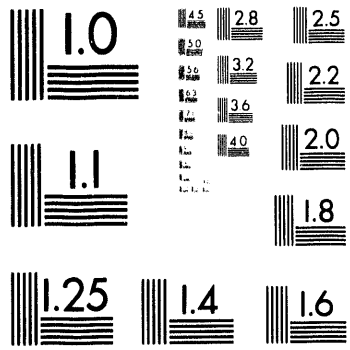
1.0
1.1
1.25
1.4
1.6
1.8
2.0
2.2
2.5
2.8
3.2
3.6
4.0
4.5
5.0

1 of 1

DEVELOPMENT OF A HIGH-PERFORMANCE COAL-FIRED POWER GENERATING SYSTEM WITH PYROLYSIS GAS AND CHAR-FIRED HIGH TEMPERATURE FURNACE (HITAF)

DE-AC22-91PC91154

Quarterly Progress Report 6

April through June 1993

Prepared for

Pittsburgh Energy Technology Center

Pittsburgh, Pennsylvania

FWDC Project 9-41-3492

August 1993

FOSTER WHEELER DEVELOPMENT CORPORATION

12 Peach Tree Hill Road, Livingston, New Jersey 07039

Contents

Figures

Figures (Cont)

Tables

QUARTERLY PROGRESS REPORT 6 (April through June 1993)

INTRODUCTION

A concept for an advanced coal-fired combined-cycle power generating system is currently being developed. The first phase of this three-phase program consists of conducting the necessary research and development to define the system, evaluating the economic and technical feasibility of the concept, and preparing an R&D plan to develop the concept further.

Foster Wheeler Development Corporation is leading a team of companies involved in this effort. The team consists of:

- AlliedSignal Aerospace Company—AiResearch Division
- Bechtel Corporation
- Research-Cottrell
- TRW, Inc.
- Foster Wheeler Energy Corporation.

The power generating system being developed in this project will be an improvement over current coal-fired systems. Goals have been specified that relate to the efficiency, emissions, costs, and general operation of the system. These goals are:

- Total station efficiency of at least 47 percent.
- No more than: 0.15 lb $NO_x/10^6$ Btu fuel heat input
  0.15 lb $SO_x/10^6$ Btu fuel heat input
  0.0075 lb of particulates/10^6 Btu fuel heat input.
- All solid wastes must be benign. Generation of solid wastes is minimized through production of usable by-products.
- Over 95 percent of the total heat input is ultimately from coal, with initial systems capable of using coal for at least 65 percent of the heat input.
- Efficient and economic baseload power generation:
  - Operation with a range of U.S. coals
  - Annual capacity factor of 65 percent
  - Load following with minimal degradation in efficiency

- Net electrical output as low as 100 MW
- 10-percent lower cost of electricity (COE) relative to a modern coal-fired plant conforming to NSPS.

- Safety, reliability, and maintainability to meet or exceed conventional coal-fired power plants.

- Amenable to construction using factory-assembled modular components based upon standard design.

The system proposed to meet these goals is a combined-cycle system where air for a gas turbine is indirectly heated to approximately 1800°F in furnaces fired with coal-derived fuels and then directly heated in a natural-gas-fired combustor to about 2400°F. The system is based on a pyrolyzing process that converts the coal into a low-Btu fuel gas and char. The fuel gas is relatively clean, and it is fired to heat tube surfaces that are susceptible to corrosion and problems from ash deposition. In particular, the high-temperature air heater tubes, which will need to be a ceramic material, will be located in a separate furnace or region of a furnace that is exposed to combustion products from the low-Btu fuel gas only. A simplified process flow diagram is shown in Figure 1.

PROJECT WORK

Task 1—Project Work Plan

The Project Work Plan was revised during this quarter and submitted to DOE.

Task 2—Conceptual Definition and Analysis

Subtask 2.7—Define Cycle Analysis Model

Plant Heat and Material Balance. The plant heat and material balance was revised during this quarter to reflect input from the team members. Of particular importance was the input from GE which officially joined the team in May. Previous balances were based on in-house data that Bechtel had for the 7FA machine. During this quarter, GE reviewed the application of the 7FA for our particular configuration and provided revised performance information. The major efforts of the changes in gas turbine data were a reduction in inlet air flow, an increase in the percentage of bypass air, and an increase in methane consumption. Fortunately, even with these changes, we were able to still meet the project goals of 47 percent efficiency and 65 percent heat input from coal.

The original balances developed assumed an inlet air rate of 3.46×10^6 lb/h. This number was based on inhouse GE data for the 7FA machine provided for other technology evaluations. For the HITAF project GE recommends a maximum air intake of 3.31×10^6 lb/h, or about 4.5 percent less flow. Since all flows around the plant, including the coal feed, are

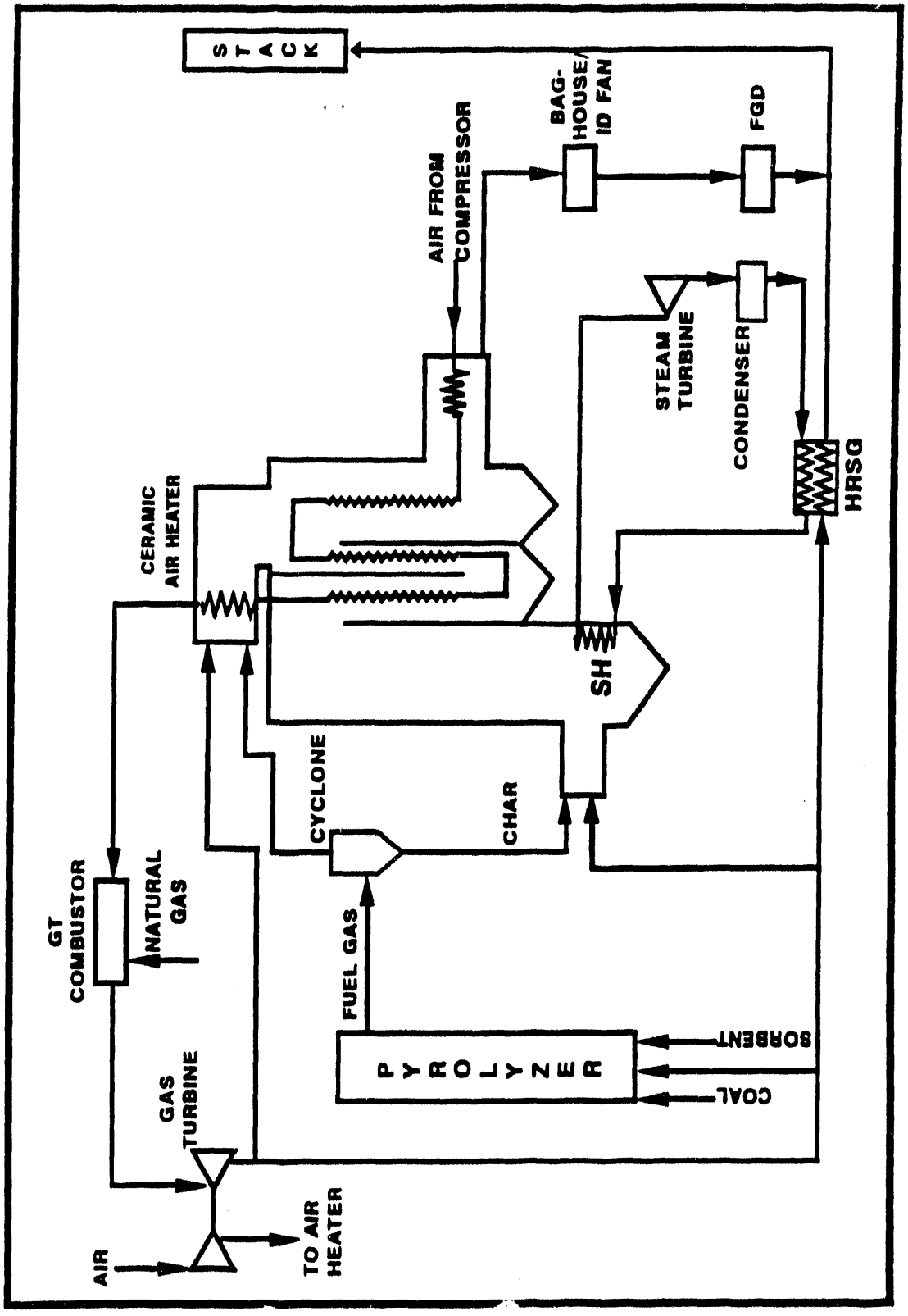

Figure 1 Simplified Process Block Flow Diagram

factored from the size of the gas turbine, this means the overall plant output and flow rates were reduced by the same percentage.

The original balance assumed a compressed air flow leaving the compressor of 2.96×10^6 lb/h, also based on Bechtel inhouse information. The new balance from GE reduced this flow to a 2.55×10^6 lb/h, a reduction of almost 14 percent. This meant the flows through the high pressure circuit were affected even more. Also, since we can still only take the air up to 1800°F, less energy can be transferred to the air from the coal (either through the combustion of the fuel gas or combustion of char) per pound of air entering the compressor. This has an adverse effect on the overall efficiency of the system.

The original balance used sufficient methane to take the combustion gas entering the turbine up to about 2425°F. After introducing the bypass cooling air and passing the first set of blades in the turbine, the temperature was a little under the 2300°F typically used for Frame 7 machines. In order to achieve the same approximate temperatures after the first set of blades, GE increased the methane flow by about 11 percent which increased the firing temperature to almost 2600°F. This increased the percentage of methane used to 34.7 percent of the total fuel fed.

In addition to these major modifications, there were also minor variations in pressures, temperatures, and performance provided by GE that have been entered into the Bechtel cycle analysis and subsequently into the July 1 balance. A summary of the heat and material balance data for the gas turbine is provided in Figure 2.

A process flow diagram is shown in Figure 3. Tables 1 and 2 are the heat and material balances issued on July 1. Table 1 is a listing of the balance maintained in a spreadsheet format. It provides a definition of the stream flows and component breakdown. Table 2 is a listing of the corresponding GATE output. There are minor differences between the spreadsheet balance and the GATE output. These reflect the variation in the method of calculation and data bases used. Other simulation programs have been used to determine which, if either, was more accurate, but the result was only additional alternatives. Since the variations are small they should not have a significant impact on the conceptual design. In general, Table 1 should be used for flow, compositions, and temperatures, while Table 2 should be used for determining heat loads on the various pieces of equipment.

The heat and material balances shown in Tables 1 and 2 do not represent the final balance for Phase 1. Minor adjustments will be made as additional information becomes available through the implementation of the conceptual design. The current material balance is judged to be sufficiently accurate to serve as the basis for starting the conceptual design.

The heat and material balances in Tables 1 and 2 also reflect changes in the location of steam superheat surfaces. The original system placed the primary superheater entirely in the hot gas portion of the high-temperature furnace. This was followed by a secondary superheater used to cool the fuel gas leaving the pyrolyzer. The final superheater was located downstream of the primary air heater.

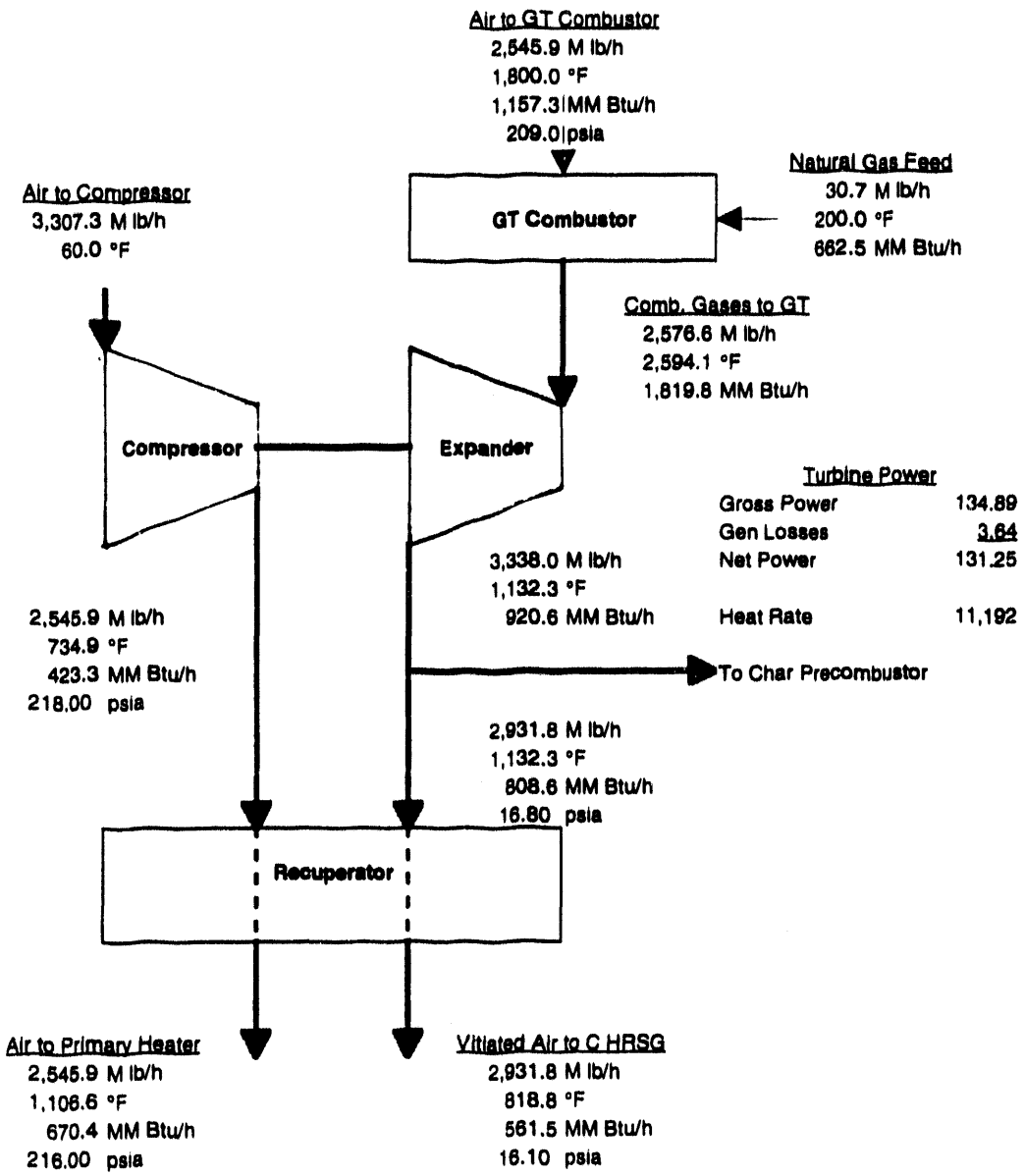

Figure 2 Gas Turbine Heat and Material Balance

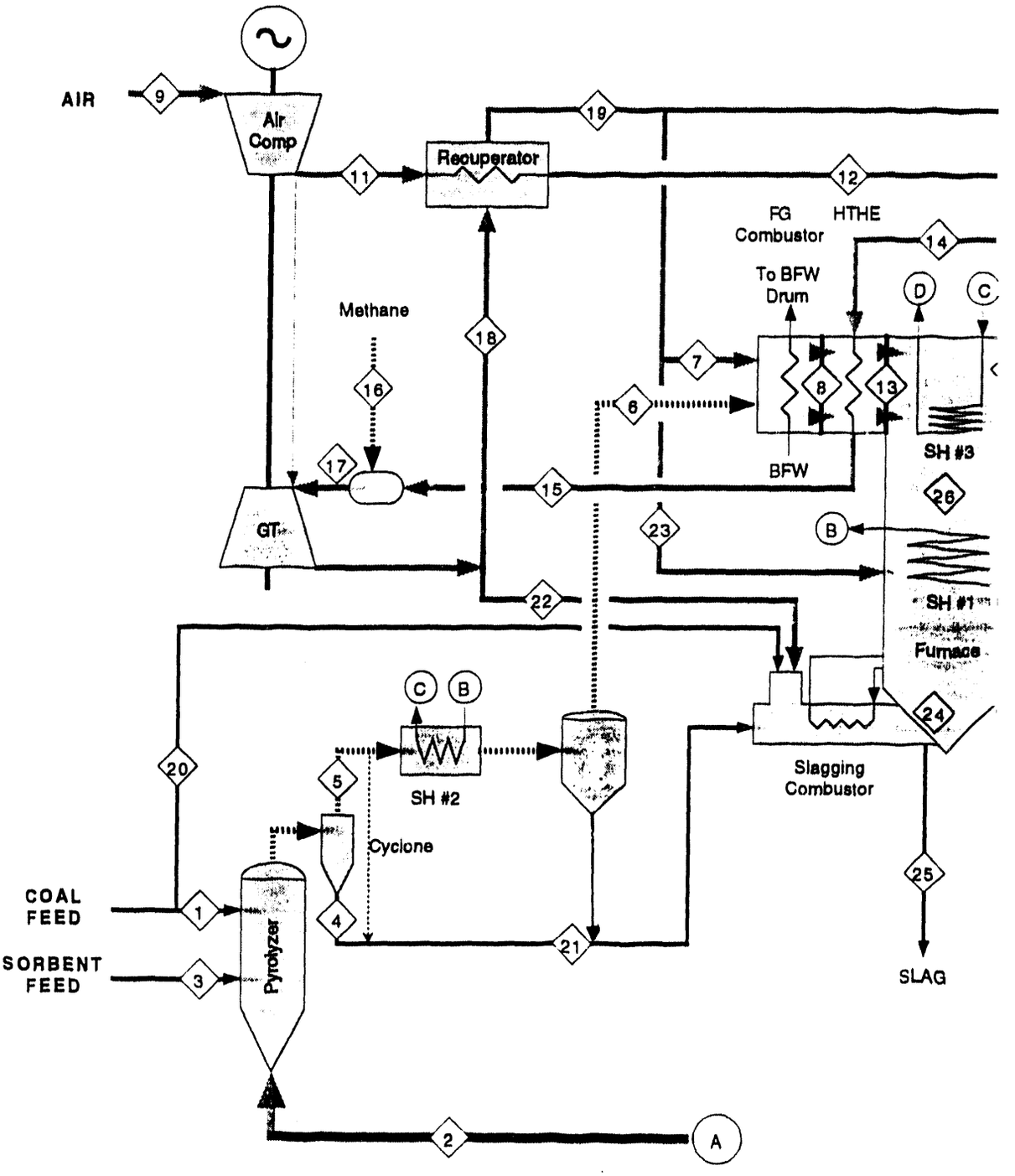
AIR
9
Air Comp
11
Recuperator
19
12
FG Combustor
HTHE
14
To BFW Drum
D
C
Methane
18
16
7
8
13
6
17
BFW
SH #3
15
26
GT
23
B
22
SH #1
Furnace
C
B
24
20
5
SH #2
Slagging Combustor
Cyclone
25
COAL FEED
1
4
21
SORBENT FEED
3
Pyrolyzer
SLAG
2
A

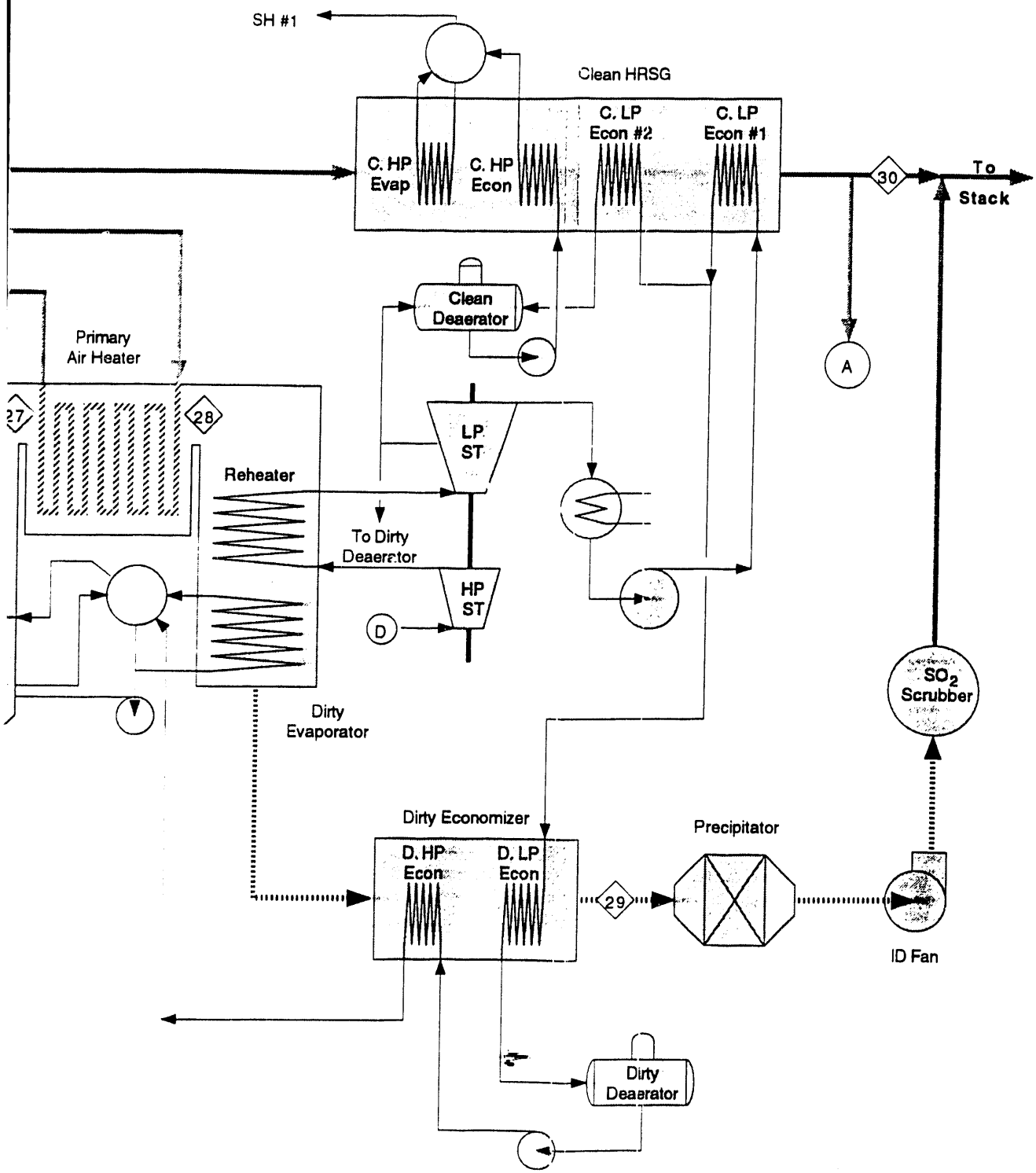

Figure 3 System Flow Diagram

Table 1 Heat and Material Balance

	Stream No.	1		2		3		4		5		6		7	
		Coal to Carbonizer		V. Air to Carbonizer		Sorbent to Carbonizer		Char fm Carbonizer		Fuel G. fm Carbonizer		Fuel Gas to Combust		V. Air to Combust	
Stream		%wt	lb/hr	%wt	lb/hr	%wt	lb/hr	%wt	lb/hr	%wt	lb/hr	%wt	lb/hr	%wt	lb/hr
	Carbon	71.92%	69,379					60.41%	26,538						
	Hydrogen	4.69%	4,524					0.38%	167						
	Oxygen	6.33%	6,102												
	Nitrogen	1.26%	1,212					1.06%	464						
	Sulfur	2.99%	2,887					1.00%	440						
Solids	Ash	10.32%	9,955			0.95%	90	22.87%	10,045						
lb/h	Moisture	2.50%	2,411			2.00%	189								
	CaCO3					95.50%	9,006								
	MgCO3					1.55%	146								
	CaO							2.26%	995						
	MgO							0.16%	70						
	CaS							11.86%	5,212						
	CaSO4														
	CH4									1.32%	4,355	1.32%	4,326		
	C2H4														
	C2H6														
	C3H8														
	CO									21.77%	72,096	21.77%	71,618		
Gases	H2									1.18%	3,918	1.18%	3,892		
lb/h	CO2			2.57%	6,523					12.28%	40,651	12.28%	40,382	2.57%	14,431
	H2O		15,608	2.88%	7,299					5.22%	17,294	5.22%	17,179	2.88%	16,147
	O2			19.07%	48,409									19.07%	107,100
	N2			74.21%	188,361					57.07%	188,999	57.07%	187,745	74.21%	416,726
	H2S									0.04%	140	0.04%	139		
	COS														
	SO2														
	C6H6+														
	Argon			1.27%	3,213					0.97%	3,213	0.97%	3,192	1.27%	7,108
	NH3									0.16%	516	0.16%	513		
	NO2														
	Total Gas, lb/h	100.00%	112,075	100.00%	253,804	100.00%	9,431	100.00%	43,930	100.00%	331,171	100.00%	328,974	100.00%	561,513
					8,790						13,454		13,364		19,447
					28.87						24.62		24.62		28.87
	Pressure, psia		49.40		32.34		34.40		29.40		29.40		29.40		29.40
	Temperature, °F		70.00		350.00		70.00		1,700.00		1,700.00		1,200.00		817.80
	Temperature, °C		21.11		176.67		21.11		926.67		926.67		648.89		436.56
	Sens. Heat, MM Btu/hr		2.82		19.94		0.02		18.74		175.84		117.60		107.40
	Lat. Heat, MM Btu/hr		16.39		7.66						18.16		18.04		16.95
	LHV, Btu/lb		12,454.70						9,502.07		1,852.34		1,852.34		
	HHV, Btu/lb		12,915.96						9,536.02		2,042.65		2,042.65		
	LHV, MM Btu/hr		1,201.47						417.43		613.44		609.37		
	HHV, MM Btu/hr		1,245.96						418.92		676.46		671.98		
Total Energy,	LHV		1,204.28		19.94		0.02		436.17		789.28		726.97		107.40
MM Btu/h,	HHV		1,265.17		27.60		0.02		437.67		870.46		807.62		124.36

Table 1 (Cont) Heat and Material Balance

	Stream No.	8		9		11		12		13		14		15	
Stream		Flue Gas to HTHE %wt	lb/hr	Air to Compressor %wt	lb/hr	Air to Recuperator %wt	lb/hr	Air to Air Heater %wt	lb/hr	Flue Gas to Furnace %wt	lb/hr	Air to HTHE %wt	lb/hr	Air to GT Combustor %wt	lb/hr
	Carbon														
	Hydrogen														
	Oxygen														
	Nitrogen														
	Sulfur														
Solids lb/h	Ash														
	Moisture														
	CaCO3														
	MgCO3														
	CaO														
	MgO														
	CaS														
	CaSO4														
	CH4														
	C2H4														
	C2H6														
	C3H8														
	CO														
Gases lb/h	H2														
	CO2	20.12%	179,206	0.05%	1,565	0.05%	1,205	0.05%	1,205	20.12%	179,206	0.05%	1,205	0.05%	1,205
	H2O	8.84%	78,710	0.82%	27,039	0.82%	20,814	0.82%	20,814	8.84%	78,710	0.82%	20,814	0.82%	20,814
	O2	1.82%	16,164	22.95%	759,147	22.95%	584,378	22.95%	584,378	1.82%	16,164	22.95%	584,378	22.95%	584,378
	N2	67.88%	604,471	74.90%	2,477,293	74.90%	1,906,976	74.90%	1,906,976	67.88%	604,471	74.90%	1,906,976	74.90%	1,906,976
	H2S														
	COS														
	SO2	0.03%	262							0.03%	262				
	C6H6+														
	Argon	1.16%	10,300	1.28%	42,256	1.28%	32,528	1.28%	32,528	1.16%	10,300	1.28%	32,528	1.28%	32,528
	NH3														
	NO2	0.16%	1,385							0.16%	1,385				
Total Gas, lb/h		100.00%	890,497	100.00%	3,307,300	100.00%	2,545,900	100.00%	2,545,900	100.00%	890,497	100.00%	2,545,900	100.00%	2,545,900
			30,558		113,693		87,519		87,519		30,558		87,519		87,519
			29.14		29.09		29.09		29.09		29.14		29.09		29.09
Pressure, psia			15.60		14.70		218.00		216.00		15.40		213.00		209.00
Temperature, °F			2,935.60		60.00		734.90		1,106.60		1,966.50		1,400.00		1,800.00
Temperature, °C			1,613.11		15.56		390.50		597.00		1,074.72		760.00		982.22
Sens. Heat, MM Btu/hr			774.47		0.79		423.31		670.37		489.93		872.77		1,157.31
Lat. Heat, MM Btu/hr			82.65		28.39		21.85		21.85		82.65		21.85		21.85
LHV, Btu/lb															
HHV, Btu/lb															
LHV, MM Btu/hr															
HHV, MM Btu/hr															
Total Energy, MM Btu/h,	LHV		774.47		0.79		423.31		670.37		489.93		872.77		1,157.31
	HHV		857.11		29.19		445.17		692.23		572.58		894.62		1,179.16

Table 1 (Cont) Heat and Material Balance

	Stream No.	16		17		18		19		20		21		22		23	
		Nat Gas to GT Comb.		FG fm GT Combustor		Gas to Recuperator		Gas fm Recuperator		Coal to Precomb.		Char to Char Comb.		Prim. Air to Char C.		Sec. Air to Char C.	
Stream		%wt	lb/hr	%wt	lb/hr	%wt	lb/hr	%wt	lb/hr	%wt	lb/hr	%wt	lb/hr	%wt	lb/hr	%wt	lb/hr
	Carbon									71.92%	6,482	57.53%	26,538				
	Hydrogen									4.69%	423	0.36%	167				
	Oxygen									6.33%	570						
	Nitrogen									1.26%	113	1.01%	464				
	Sulfur									2.99%	270	0.95%	440				
Solids	Ash									10.32%	930	21.78%	10,045				
lb/h	Moisture									2.50%	225						
	CaCO3																
	MgCO3																
	CaO											2.16%	995				
	MgO											0.15%	70				
	CaS											11.30%	5,212				
	CaSO4																
	CH4	100.00%	30,701									0.06%	29				
	C2H4																
	C2H6																
	C3H8																
	CO											1.04%	478				
Gases	H2											0.06%	26				
lb/h	CO2			3.32%	85,427	2.57%	75,347	2.57%	75,347			0.58%	270	2.57%	10,440	2.57%	5,220
	H2O			3.48%	89,766	2.88%	84,309	2.88%	84,309			0.25%	115	2.88%	11,682	2.88%	5,841
	O2			17.93%	461,904	19.07%	559,192	19.07%	559,192					19.07%	77,481	19.07%	38,741
	N2			74.01%	1,906,976	74.21%	2,175,814	74.21%	2,175,814			2.72%	1,254	74.21%	301,480	74.21%	150,740
	H2S											0.00%	1				
	COS																
	SO2																
	C6H6+																
	Argon			1.26%	32,528	1.27%	37,114	1.27%	37,114			0.05%	21	1.27%	5,142	1.27%	2,571
	NH3											0.01%	3				
	NO2																
Total Gas, lb/h		100.00%	30,701	100.00%	2,576,601	100.00%	2,931,776	100.00%	2,931,776	100.00%	9,013	100.00%	46,127	100.00%	406,225	100.00%	203,113
			1,914		89,433		101,538		101,538						14,069		7,035
			16.04		28.81		28.87		28.87						28.87		28.87
	Pressure, psia		250.00		191.70		16.80		16.10		16.80				16.80		
	Temperature, °F		200.00		2,594.10		1,132.30		818.80		60.00		1,700.00		1,132.30		818.80
	Temperature, °C		93.33		1,423.39		611.28		437.11		15.56		926.67		611.28		437.11
	Sens. Heat, MM Btu/hr		2.38		1,819.81		808.58		561.54		0.00		24.98		112.04		38.90
	Lat. Heat, MM Btu/hr				94.25		88.52		88.52						12.27		6.13
	LHV, Btu/lb		21,502.00								12,454.70		9,137.78				
	HHV, Btu/lb		23,861.00								12,915.96		9,179.19				
	LHV, MM Btu/hr		660.13								112.26		421.50				
	HHV, MM Btu/hr		732.56								116.41		423.41				
Total Energy,	LHV		662.52		1,819.81		808.58		561.54		112.26		446.48		112.04		38.90
MM Btu/h,	HHV		734.94		1,914.06		897.11		650.07		116.42		448.39		124.30		45.04

Table 1 (Cont) Heat and Material Balance

	Stream No.	24		25		26		27		28		29		30		31	
		FG to DSH #1-A		Slag fm Char Comb.		FG to SH #3		Tot Gas to Air Htr.		F. Gas fm Air Htr.		Dirty FG to FGD		Clean FG fm LP Econ		F. Gas to Stack	
Stream		%wt	lb/hr	%wt	lb/hr	%wt	lb/hr	%wt	lb/hr	%wt	lb/hr	%wt	lb/hr	%wt	lb/hr	%wt	lb/hr
	Carbon																
	Hydrogen																
	Oxygen																
	Nitrogen			3.40%	577												
	Sulfur																
Solids	Ash			64.62%	10,975												
lb/h	Moisture																
	CaCO3																
	MgCO3																
	CaO			23.21%	3,942												
	MgO			0.41%	70												
	CaS			8.36%	1,421												
	CaSO4																
	CH4																
	C2H4																
	C2H6																
	C3H8																
	CO																
Gases	H2																
lb/h	CO2	21.28%	137,751			21.28%	137,751	20.61%	316,956	20.61%	316,956	20.61%	316,956	2.57%	55,696	10.61%	366,130
	H2O	3.39%	21,943			3.39%	21,943	6.55%	100,654	6.55%	100,654	6.55%	100,654	2.88%	62,321	4.51%	155,676
	O2	3.34%	21,629			3.34%	21,629	2.46%	37,793	2.46%	37,793	2.46%	37,793	19.07%	413,351	11.67%	402,735
	N2	70.06%	453,473			70.06%	453,473	68.80%	1,057,944	68.80%	1,057,944	68.80%	1,057,944	74.21%	1,608,348	71.80%	2,477,931
	H2S																
	COS																
	SO2	0.74%	4,786			0.74%	4,786	0.33%	5,048	0.33%	5,048	0.33%	5,048			0.15%	5,048
	C6H6+																
	Argon	1.19%	7,714			1.19%	7,714	1.17%	18,014	1.17%	18,014	1.17%	18,014	1.27%	27,434	1.22%	42,235
	NH3																
	NO2	0.00%	9			0.00%	9	0.09%	1,395	0.09%	1,395	0.09%	1,395			0.04%	1,395
Total Gas, lb/h		100.00%	647,305	100.00%	16,985	100.00%	647,305	100.00%	1,537,802	100.00%	1,537,802	100.00%	1,537,802	100.00%	2,167,151	100.00%	3,451,149
			21,287				21,287		51,845		51,845		51,845		75,056		118,111
			30.41				30.41		29.66		29.66		29.66		28.87		29.22
	Pressure, psia		15.80		15.80		15.70		15.50		15.00		15.00		15.00		14.70
	Temperature, °F		3,234.80		2,400.00		2,687.00		1,906.30		1,389.10		220.00		130.00		220.00
	Temperature, °C		1,779.33		1,315.56		1,475.00		1,041.28		753.94		104.44		54.44		104.44
	Sens. Heat, MM Btu/hr		594.67		17.99		482.26		799.28		556.81		61.83		37.61		137.28
	Lat. Heat, MM Btu/hr		23.04				23.04		105.69		105.69		105.69		65.44		163.46
	LHV, Btu/lb																
	HHV, Btu/lb																
	LHV, MM Btu/hr																
	HHV, MM Btu/hr																
Total Energy,	LHV		594.67		17.99		482.26		799.28		556.81		61.83		37.61		137.28
MM Btu/h,	HHV		617.71		17.99		505.30		904.97		662.49		167.51		103.05		300.74

Table 2 GATE Output

	Flow M lb/hr	Temp °F	Press psia	Enthalpy Btu/lb	Power MWe	Duty MM Btu/hr
Air Compressor					162.10	
Inlet	3,307.30	60.0	14.5			
Outlet	3,307.30	734.9	227.4	167.2		
Air Heater Recuperator after GT						248.03
Hot - In	2,929.50	1,132.3	16.8	277.2		
Hot - Out	2,929.50	817.8	16.1	192.4		
Cold - In	2,546.50	734.9	227.4	167.2		
Cold - Out	2,546.50	1,106.6	226.1	264.6		
Furnace Air Heater						203.21
Hot - In	1,537.60	1,905.0	15.4	523.7		
Hot - Out	1,537.60	1,476.2	15.4	391.2		
Cold - In	2,546.50	1,106.6	226.1	264.6		
Cold - Out	2,546.50	1,400.0	221.1	344.4		
High Temp. Air Heater						286.74
Hot - In	886.97	2,929.9	15.6	869.3		
Hot - Out	886.97	1,941.2	15.5	545.5		
Cold - In	2,546.50	1,400.0	221.1	344.4		
Cold - Out	2,546.50	1,800.0	212.3	457.0		
Duct Burner for NG						
Gas - In	2,546.50	1,800.0	212.3	457.0		
Gas - Out	2,577.20	2,593.2	203.8	708.5		
Fuel	30.70	200.0	195.0			
GATE Gas Turbine Expander					299.80	
Inlet	2,577.20	2,593.2	203.8	708.5		
Outlet	3,337.99	1,132.3	16.8	277.2		
Cooling	760.79	734.9	227.4	167.2		
HRSG Boiler						55.67
Gas - In	2,162.50	817.8	16.1	192.4		
Gas - Out	2,162.50	719.8	15.5	166.6		
BFW - In	180.81	672.7	2,948.1	730.2		
Stm - Out	180.81	890.7	2,909.8	1,038.1		
Clean HP Econ.						199.73
Gas - In	2,162.50	719.8	15.5	166.6		
Gas - Out	2,162.50	359.0	15.1	74.1		
BFW - In	445.62	306.9	2,865.0	282.0		
BFW - Out	445.62	672.7	2,836.4	730.2		
2nd Stage of Clean Econ. (C Econ #2)						53.14
Gas - In	2,162.50	359.0	15.1	74.1		
Gas - Out	2,162.50	260.5	15.0	49.5		
BFW - In	445.03	181.0	79.4	149.2		
BFW - Out	445.03	296.9	78.6	268.6		

Table 2 GATE Output (Cont)

	Flow M lb/hr	Temp °F	Press psia	Enthalpy Btu/lb	Power MWe	Duty MM Btu/hr
Clean LP Economizer						69.77
Gas - In	2,162.50	260.5	15.0	49.5		
Gas - Out	2,162.50	130.0	14.2	17.2		
BFW - In	837.58	97.7	80.0	65.9		
BFW - Out	837.58	181.0	79.4	149.2		
Vitiated Air Booster for Pyrolyzer						
Inlet	253.82	130.0	14.2	17.2	2.79	
Outlet	253.82	261.5	29.9	54.7		
2nd Stage of Superheater (SH #2)						52.18
Stm - In	841.61	750.0	2,649.5	1,236.2		
Stm - Out	841.61	805.2	2,649.5	1,298.2		
Pyrogas burner						
Gas - In	562.79	617.8	16.1	192.4		
Gas - Out	886.97	3,145.5	15.8	938.9		
Fuel	324.18	1,213.1	23.8			
Boiler-4, SG Burner Cooling						61.64
Gas - In	886.97	3,145.5	15.8	938.9		
Gas - Out	886.97	2,929.9	15.6	869.3		
BFW - In	200.21	672.7	2,836.4	730.2		
Stm - Out	200.21	690.7	2,799.5	1,038.1		
SG Precombustor						
Gas - In	408.48	1,132.3	16.8	277.2		
Gas - Out	410.65	1,168.4	16.7	287.4		
Fuel	2.17	1,213.1	20.0			
Coal Precombustor						
Inlet	410.65	1,168.4	16.7	287.4		
Outlet	416.73	2,042.4	16.6	546.5		
Fuel	6.08	196.3	25.0			
Boiler-1 for Cooling Precombustor						3.20
Gas - In	416.73	2,042.4	16.6	546.5		
Gas - Out	416.73	2,017.1	16.5	536.8		
BFW - In	10.40	672.7	2,836.4	730.2		
Stm - Out	10.40	690.7	2,799.5	1,038.1		
2nd Air to Slagging Comb. - Mixer						
Inlet - 1	416.73	2,017.1	16.5	536.8		
Inlet - 2	204.24	617.8	16.1	192.4		
Outlet	622.97	1,643.1	16.1	425.2		
1st Char Burner						
Gas - In	622.97	1,643.1	16.1	425.2		
Gas - Out	640.97	3,024.5	15.9	850.6		
Fuel	18.00	894.0	20.0			

Table 2 GATE Output (Cont)

	Flow M lb/hr	Temp °F	Press psia	Enthalpy Btu/lb	Power MWe	Duty MM Btu/hr
Slagging Combustor Boiler-2						95.38
Gas - In	640.97	3,024.5	15.9	850.6		
Gas - Out	640.97	2,536.6	15.8	701.5		
BFW - In	297.70	672.7	2,946.1	730.2		
Stm - Out	297.70	686.8	2,834.4	1,060.6		
2nd Char Burner						
Gas - In	640.97	2,536.6	15.8	701.5		
Gas - Out	643.97	2,756.9	15.8	770.8		
Fuel	3.00	894.0	20.0			
Superheater 1st Stage (SH #1A)						104.53
Gas - In	643.97	2,756.9	15.8	770.8		
Gas - Out	643.97	2,231.0	15.6	608.1		
Stm - In	841.61	696.7	2,794.9	1,112.0		
Stm - Out	841.61	750.0	2,649.5	1,236.2		
3rd Char Burner (CO Burner)						
Gas - In	643.97	2,231.0	15.6	608.1		
Gas - Out	650.58	2,712.4	15.6	760.2		
Fuel	6.61	894.0	20.0			
3rd Stage of SH (SH#3)						172.95
Gas - In	650.58	2,712.4	15.6	760.2		
Gas - Out	650.58	1,852.8	15.4	493.9		
Stm - In	841.61	606.2	2,649.5	1,298.2		
Stm - Out	841.61	1,075.1	2,615.1	1,503.7		
Comb. Products Mix in Furnace						
Inlet - 1	650.58	1,852.8	15.4	493.9		
Inlet - 2	886.97	1,941.2	15.5	545.5		
Outlet	1,537.55	1,905.0	15.5	523.7		
Superheater 1st Stage (SH #1B)						37.45
Gas - In	1,537.60	1,476.2	15.4	391.2		
Gas - Out	1,537.60	1,396.2	15.4	366.8		
Stm - In	841.61	686.3	2,820.2	1,067.5		
Stm - Out	841.61	696.7	2,794.9	1,112.0		
Reheater						210.29
Gas - In	1,537.60	1,396.2	15.4	366.8		
Gas - Out	1,537.60	925.0	15.4	229.8		
Stm - In	841.61	619.4	471.9	1,313.1		
Stm - Out	841.61	1,075.1	420.0	1,563.0		
Superheater 1st Stage (SH #1C)						21.04
Gas - In	1,537.60	925.0	15.4	229.8		
Gas - Out	1,537.60	876.4	15.4	216.1		
Stm - In	841.61	686.8	2,834.4	1,042.5		
Stm - Out	841.61	686.3	2,820.2	1,067.5		

Table 2 GATE Output (Cont)

	Flow M lb/hr	Temp °F	Press psia	Enthalpy Btu/lb	Power MWe	Duty MM Btu/hr
Additional Boiler after Reheat						46.95
Gas - In	1,537.60	676.4	15.4	216.1		
Gas - Out	1,537.60	766.5	15.3	185.5		
BFW - In	152.50	672.7	2,948.1	730.2		
Stm - Out	152.50	690.7	2,909.8	1,038.1		
Dirty HP Economizer						177.32
Gas - In	1,537.60	766.5	15.3	185.5		
Gas - Out	1,537.60	336.0	15.2	70.0		
BFW - In	395.99	307.1	2,977.9	282.4		
BFW - Out	395.99	672.7	2,948.1	730.2		
Dirty LP Economizer						43.61
Gas - In	1,537.60	336.0	15.2	70.0		
Gas - Out	1,537.60	224.5	15.0	41.5		
BFW - In	392.55	181.0	79.4	149.2		
BFW - Out	392.55	290.9	78.6	260.3		
FGD System						
Inlet	1,537.60	224.1	15.1	41.4		
Outlet	1,537.60	129.5	14.9	17.4		
To Stack	3,446.20	129.8	14.2	17.3		
High Press ST					47.00	
Inlet	841.61	1,075.1	2,615.1	1,503.7		
Outlet	841.61	619.2	471.9	1,313.1		
Low Press ST					126.70	
Inlet	841.51	1,075.1	420.0	1,563.0		
Outlet	816.51	98.6	0.9	1,036.8		
Extraction	25.00	844.7	172.5	1,449.5		
Condenser						790.57
Stm - In	816.51	98.6	0.9	1,036.8		
Cond - Out	816.51	98.6	0.9	66.6		
CW - In	46,829.00	63.0	15.0	31.1		
CW - Out	46,829.00	80.0	15.0	48.0		
Condensate Pump					0.07	
Wtr - In	837.58	97.6	0.9	65.7		
Wtr - Out	837.58	97.7	80.0	66.0		
Clean Deaerator						
BFW - In	445.95	298.9	78.6	268.6		
BFW - Out	446.55	300.9	70.0	270.7		
Aux - In	1.47	844.7	172.5	1,449.5		
Stm - Out	0.88	302.9	70.0	1,180.6		
Dear Pump HRST					1.38	
Wtr - In	445.62	300.9	70.0	270.7		
Wtr - Out	445.62	307.1	2,978.2	282.4		

Table 2 GATE Output (Cont)

	Flow M lb/hr	Temp °F	Press psia	Enthalpy Btu/lb	Power MWe	Duty MM Btu/hr
Dirty Deaerator						
BFW - In	392.55	290.9	78.6	260.3		
BFW - Out	395.99	300.9	70.0	270.7		
Evap - In	3.46	644.7	172.5	1,449.5		
Stm - Out	0.02	302.9	70.0	1,180.6		
Dear. Pump F					1.37	
Wtr - In	395.99	300.9	70.0	270.7		
Wtr - Out	395.99	307.1	2,865.0	282.4		

The revised version takes into account the fact that the walls throughout the entire furnace must be cooled by superheated steam to maintain proper temperatures. Therefore, Superheater No. 1 extends throughout the furnace and the new balance divides the loads based on FWEC's recommendations. Superheater No. 2 is still used to cool the fuel gas going to the fuel gas combustor but Superheater No. 3 has been placed upstream of the primary air heater to reduce the gas temperature and thereby the primary air heater metal temperature. A summary of the flows and temperatures around the fuel gas combustor and high-temperature furnace is presented in Figure 4.

The heat and material balance around the ceramic air heater has also changed due to the changes in flows. The new flow and temperature conditions around the ceramic air heater are shown in Figure 5.

In addition to the gas turbine, high-temperature furnace, and high-temperature exchanger flow diagrams presented in Figures 3, 4, and 5, Bechtel also prepared a mini-balance around the clean and dirty HRSGs. These are shown in Figures 6 and 7. The only modification made in these systems from the earlier balance is the use of the entire condensate stream in the first stage clean low-pressure economizer. The stream is then split and follows parallel paths through the remainder of the clean and dirty HRSG systems. This change accomplishes two purposes:

- It provides the ability to achieve lower temperatures in the clean gas outlet, now set at 130°F. This is lower than traditional flue gas systems because of the clean nature of the exit gas. It is still about 50°F above the estimated dew point.

- It balances the temperature profile in the two HRSGs. In the old scheme the high-pressure dirty economizer was considerably larger than the clean side due to the tight temperature approach used. Since the dirty side will likely require more expensive materials of construction, it was deemed prudent to balance the temperatures to at least make the sizes of the two HRSGs proportional to the heat being transferred.

New Plant Layout Drawings. The fuel gas furnace, ceramic exchangers, and high-temperature furnace were sufficiently defined during the current quarter to allow FWDC and FWEC to develop a preliminary configuration for these major pieces. Bechtel used the sketches developed for these systems, along with other sketches on the gas turbine, pyrolyzer, and recuperator, to develop the preliminary view of the overall plant layout displayed in Figure 8.

This version is expected to be reasonably close to the final layout to be used in the conceptual design. The placement of the major pieces should remain fairly stable although the routing of some of the major lines may require further work. Nevertheless, the layout in Figure 8 is seen to be sufficiently complete to allow initial definition of line sizes, routings, and lengths. This information will be used to calculate pressure drops for incorporation into the cycle analysis.

Overall Plant Performance. A revised analysis of the overall plant performance was made based on the heat and material balances presented in Tables 1 and 2. The result summarized

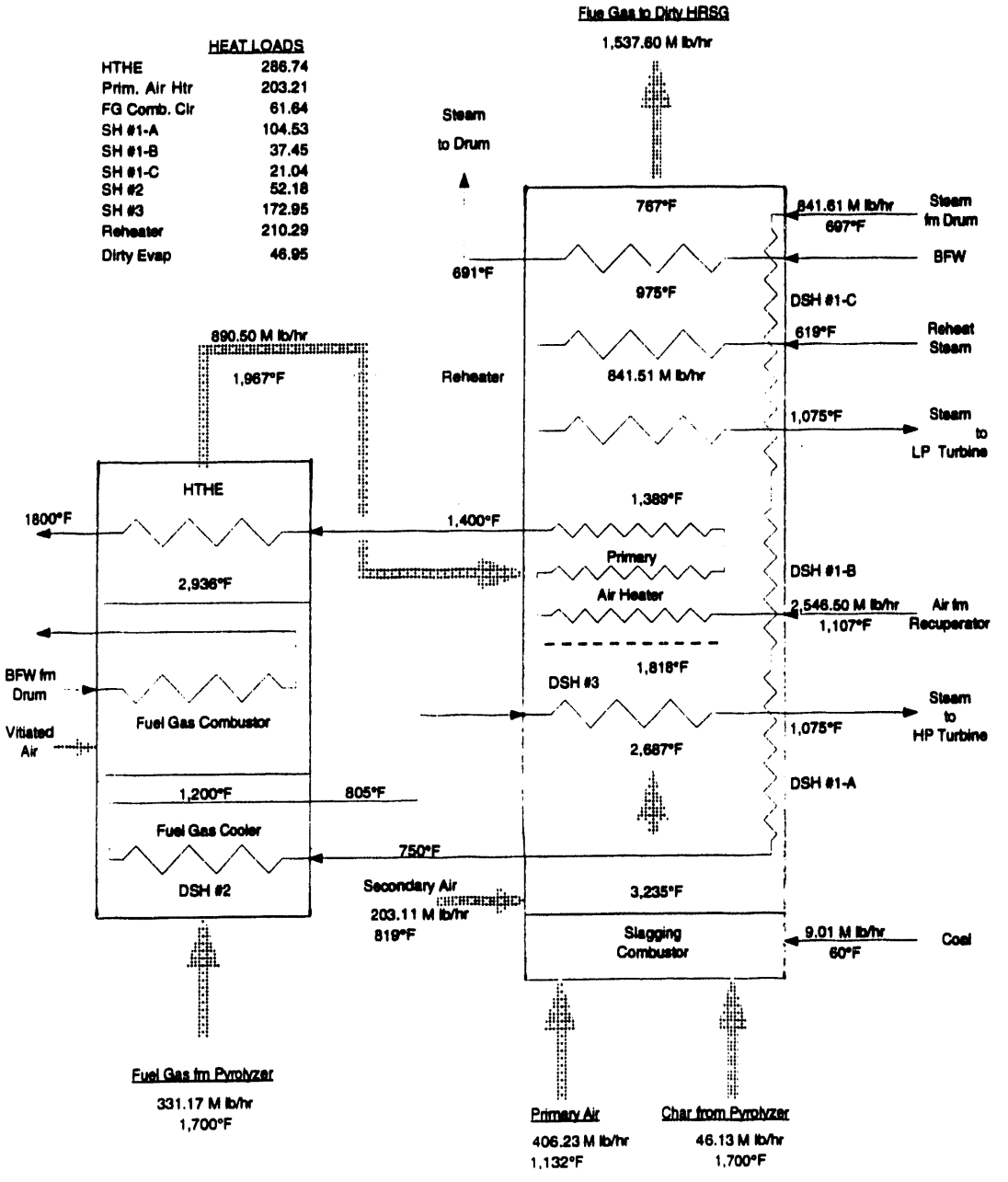

Figure 4 Superheater Arrangement

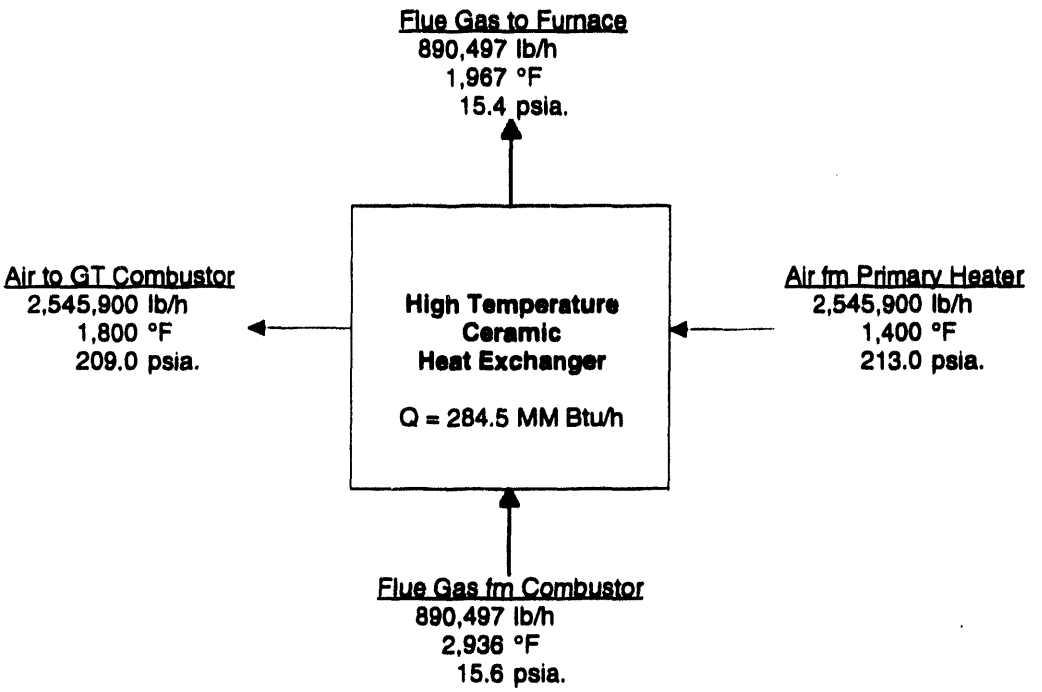

Figure 5 Ceramic Air Heater Heat and Material Balance

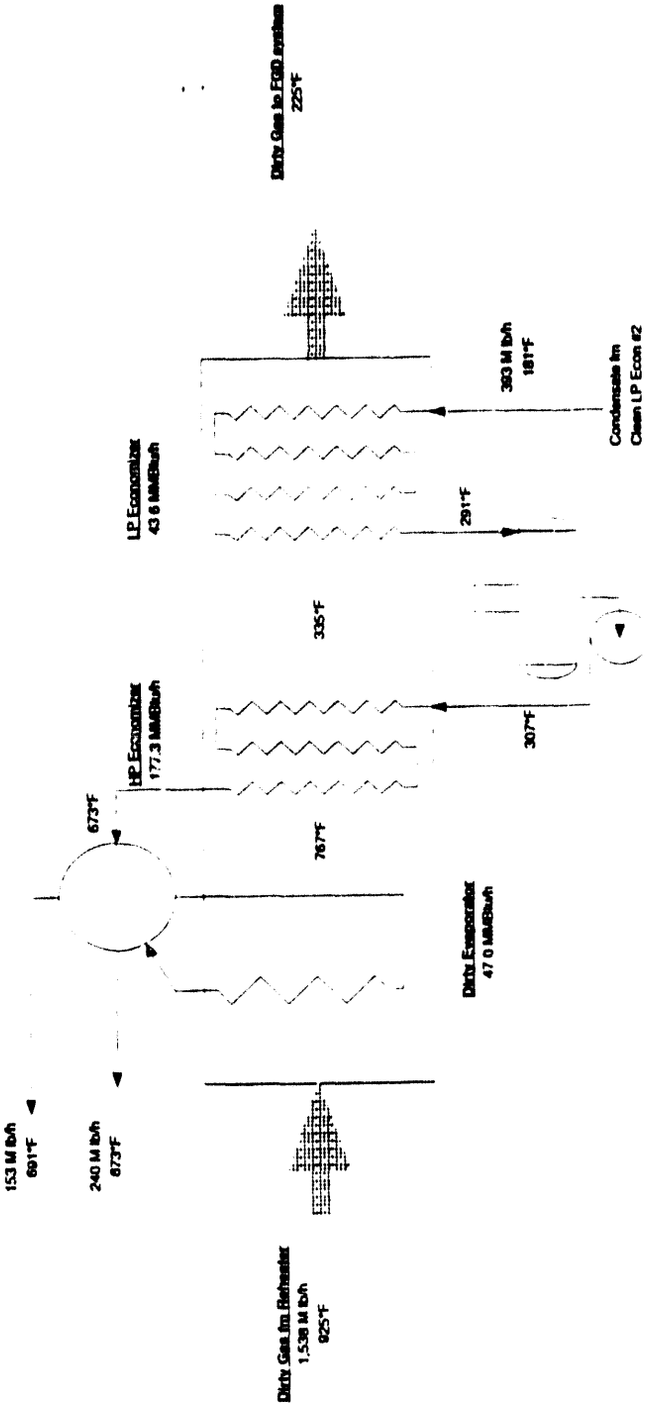

Figure 6 Dirty HRSG Heat and Material Balance

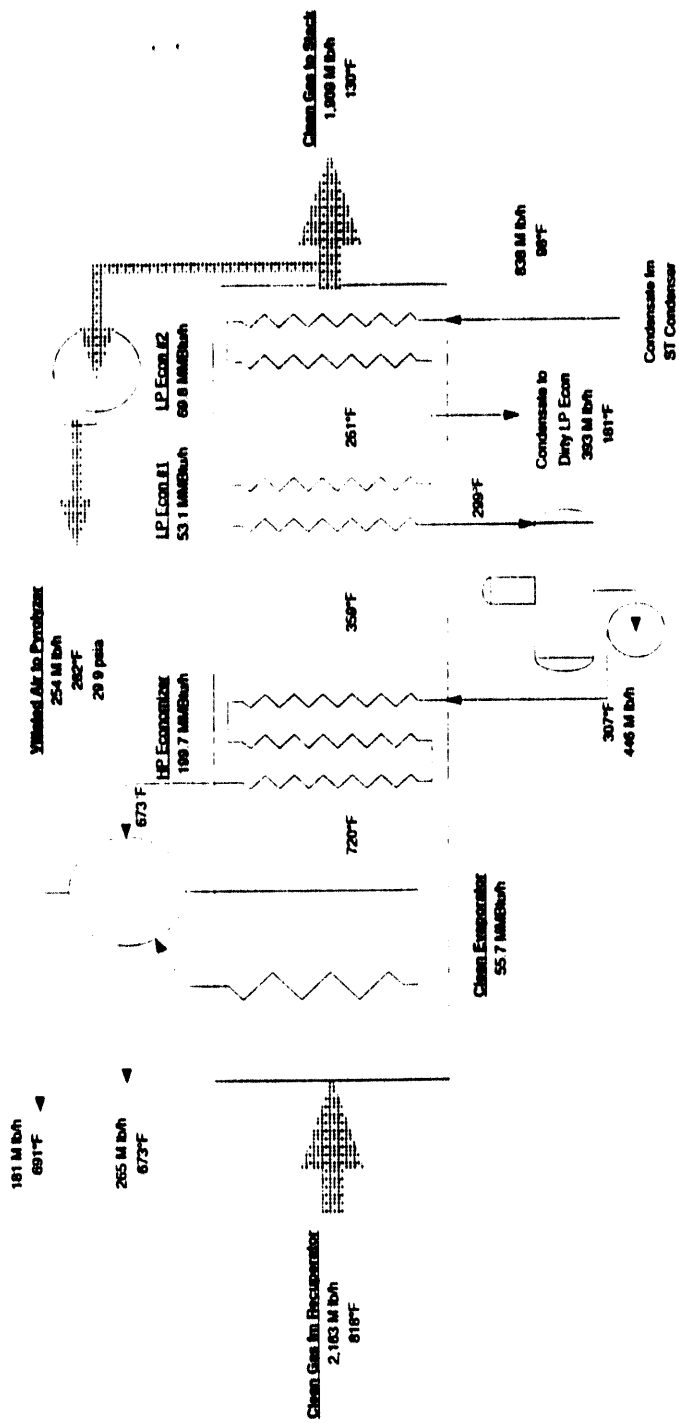

Figure 7 HRSG Heat and Material Balance

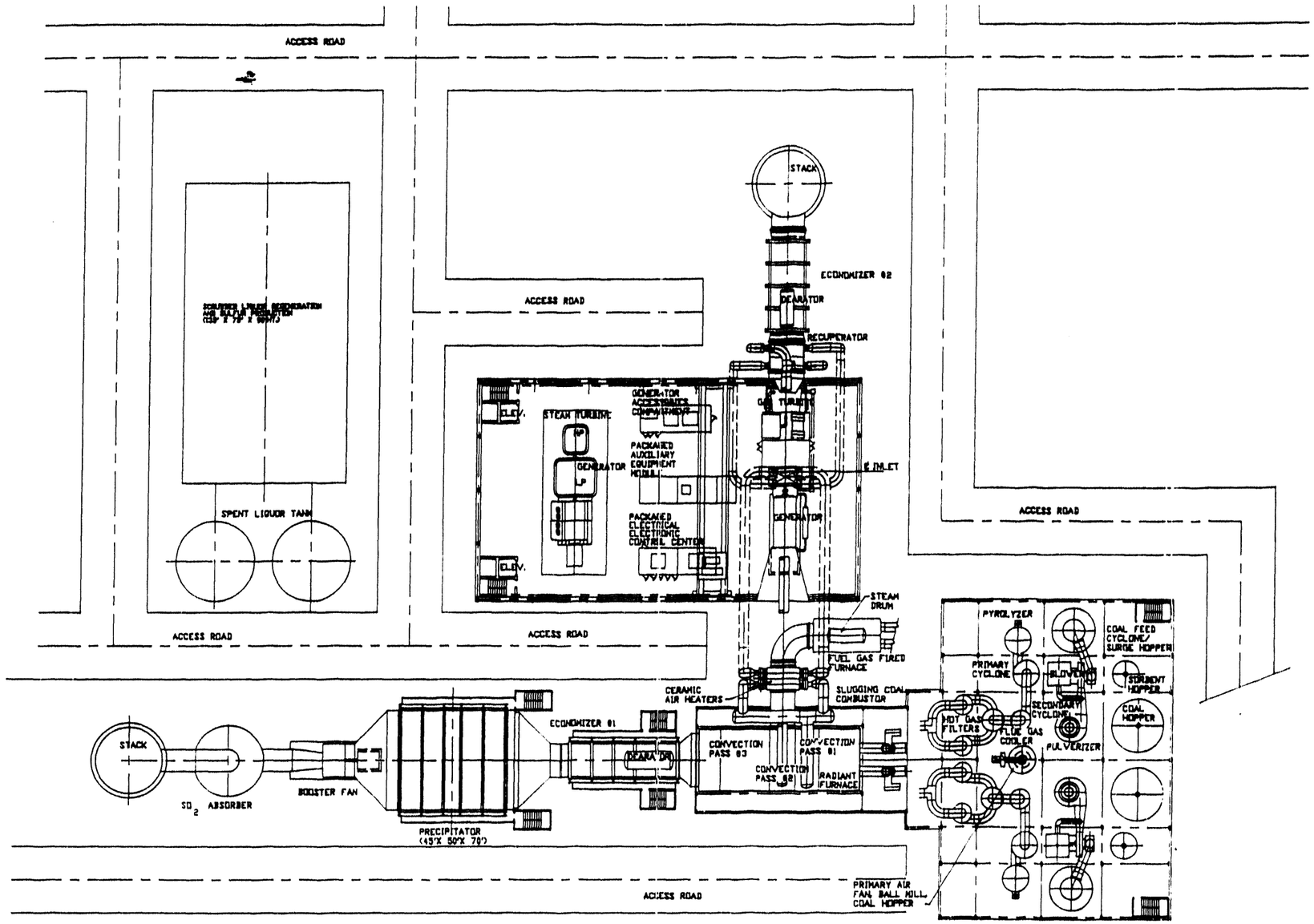

Figure 8 Preliminary Plant Layout

in Table 3 shows we are still achieving the goal of 47 percent overall efficiency based on higher heating value (HHV) and that we are using less than 35 percent of the fuel in the form of methane, but we are very close to both.

Task 3—Preliminary R&D

Subtask 3.1—Analytical Determination of Pyrolyzer Yields

Expected pyrolyzer heat and material balances have been previously reported [1]. These balances were developed using a combination of analytical models and data from the FWEC second-generation PFB pilot plant carbonizer. The Institute of Gas Technology (IGT) is currently organizing this information into one program and writing a report that will provide back-up information on the correlations used in the code. This report should be issued by the end of October.

Subtask 3.2—Characterization of Ceramic Air Heater Gas-Side Environment

The gas-side environment is an important consideration in the choice of material for the ceramic air heater and the design of the pyrolyzer subsystem. Three candidate materials have been selected for evaluation. These materials are sintered alpha-SiC, siliconized-SiC, and SiC_p/Al_2O_3 composite. The sintered alpha SiC and siliconized SiC were selected primarily based on considerations of allowable operating temperature, creep resistance, and thermal conductivity [2]. The SiC_p/Al_2O_3 composite was included primarily because of reports of resistance to alkali corrosion [3]. All three materials have experienced corrosion under certain test conditions that has been attributed to effects of alkali interactions [4,5,6].

With our HIPPS concept, the flue gas going through the ceramic air heater can essentially be made as free of alkalies as required. It is a matter of how much treatment is done to the fuel gas to remove particulates and gaseous phase alkalies. There is potentially a trade-off between fuel gas cleanup and choice of air heater material although the limited range of material characteristics and other design and operational considerations have narrowed the cleanup system choices.

A schematic of the pyrolyzer subsystem is shown in Figure 9. The subsystem consists of a circulating bed pyrolyzer, secondary cyclone, fuel gas cooler, and barrier filter. Two of these trains would be used in a 290-MW plant, but the solids flow rates shown are totals for the plant. These flow rates are based on the 12/15/92 plant heat and material balances. The stream leaving the top of the primary cyclone contains the fuel gas and the char that goes to the char combustors. Most of the char for the char combustors is separated from the fuel gas in the secondary cyclone. The fuel gas leaving the secondary cyclone still has a significant level of entrained char and gaseous phase alkalies.

In order to get an estimate of the gaseous phase alkalies, a chemical fractionation technique was used to determine the organically bound, water-soluble, and carbonate forms of the alkalies in the raw coal. It is only these forms of alkalies that have the potential to be released

Table 3 Summary of Performance

			HHV	LHV
Coal to Pyrolyzer	lb/h 10^6 Btu/h	96,467	1,265	1,204
Coal to Char Burner	lb/h 10^6 Btu/h	9,013	116	112
Natural Gas	lb/h 10^6 Btu/h	30,701	735	663
Total In	10^6 Btu/h		2,117	1,979
Gas Turbine	kWe		131.2	
Steam Turbine	kWe		168.7	
Gross Power	kWe		299.9	
Auxiliary Power Required	kWe		7.7	
Net Power	kWe		292.2	
Heat Rate	Btu/kW		7,242	6,772
Efficiency	%	47.13	50.40	

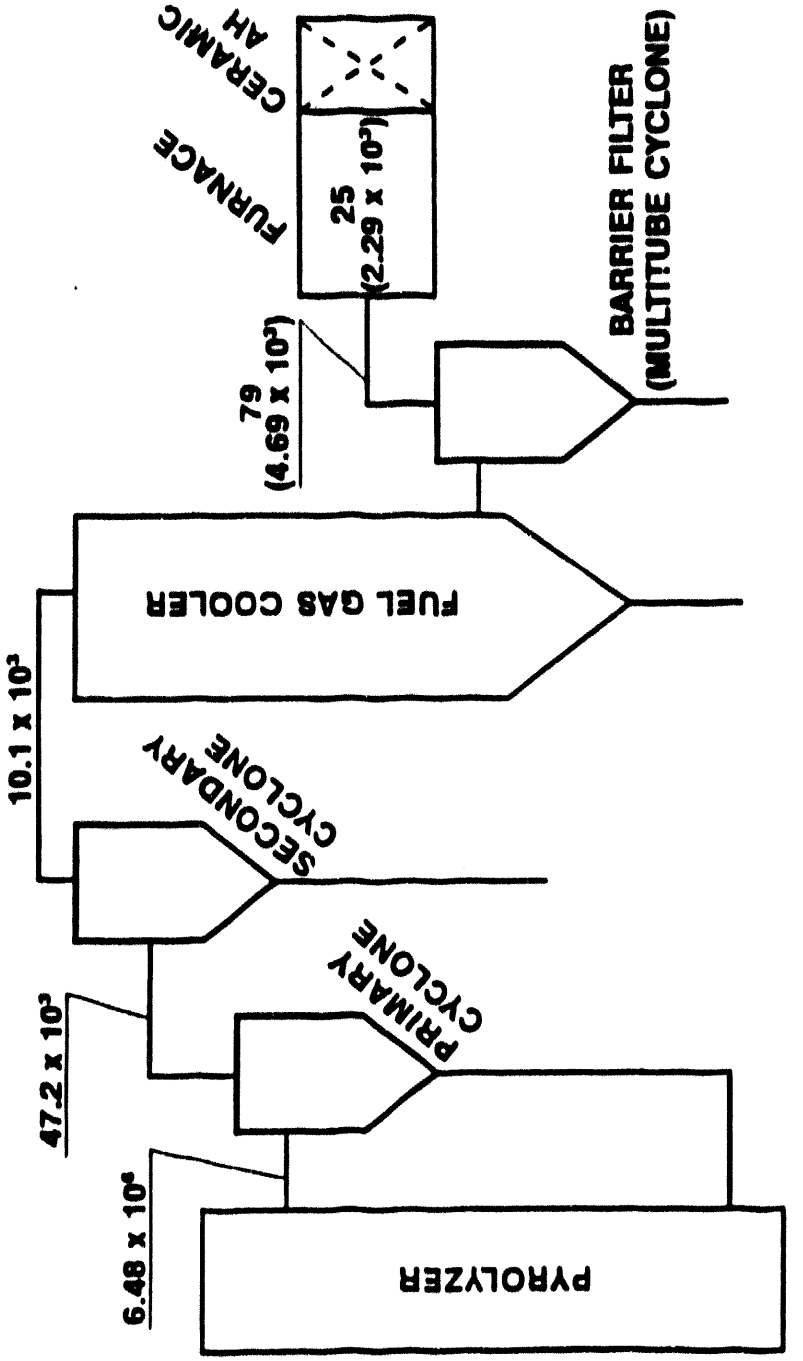

Figure 9 NG-HITAF—Particulates in Fuel Gas Stream [Total for 290-MW Plant (lb/h)]

into the fuel gas. The alkalies that are present in the coal as clays will generally not be released during the pyrolyzation process [7]. The gaseous phase alkalies estimated in this manner constitute a worst-case analysis, because total release of the soluble alkalies is assumed and gettering of the alkalies by the ash is not considered. The alkalies estimated with this analysis were included in the fuel gas composition and a thermodynamic equilibrium program was run to determine the gaseous phase alkali levels at different fuel-gas temperatures.

This procedure and the results are discussed in more detail in Quarterly Report 3 [8]. The plot of sodium concentration versus fuel-gas temperature from that analysis is shown in Figure 10. The program used for the Thermodynamic Analysis is SOLGAS MIX. It can be seen in Figure 10 that the sodium content of the fuel gas can be reduced substantially by cooling the fuel gas a few hundred degrees. It should also be noted that since this concentration is before combustion, the sodium level will be further reduced when it is diluted with the combustion air.

An important aspect of the ceramic air heater environment is the composition and deposition rate of particles that are not removed from the fuel gas. The solids flow rates shown in Figure 9 are based on a FWEC circulating bed computer model [9] and API correlations for cyclone fractional efficiency [10]. This analysis of particle carryover and deposition including assumptions is discussed in Quarterly Report 4 [11].

The information developed on fuel gas alkali concentration and ash deposition rate was used to establish test conditions for laboratory tests of the candidate ceramic materials. These tests are discussed in Subtask 3.8. As the design of the system has developed, there have been changes that may affect these analyses. These effects should be relatively minor, but the analyses will be repeated with the final system design and plant heat and material balance.

Subtask 3.8—Evaluation of Secondary Air Heater Corrosion

Laboratory corrosion tests are being run with three types of ceramics. The materials and their manufacturers are listed in Table 4.

Table 4 Candidate Secondary Air Heater Materials

Name	Manufacturer	Type of Material
Hexaloy SA	Carborundum	Alpha Sintered SiC
Silicon Carbide Particulate—Reinforced Alumina	Dupont Lanxide	SiC_p/Al_2O_3 Composite
NT-230	Norton	Siliconized SiC

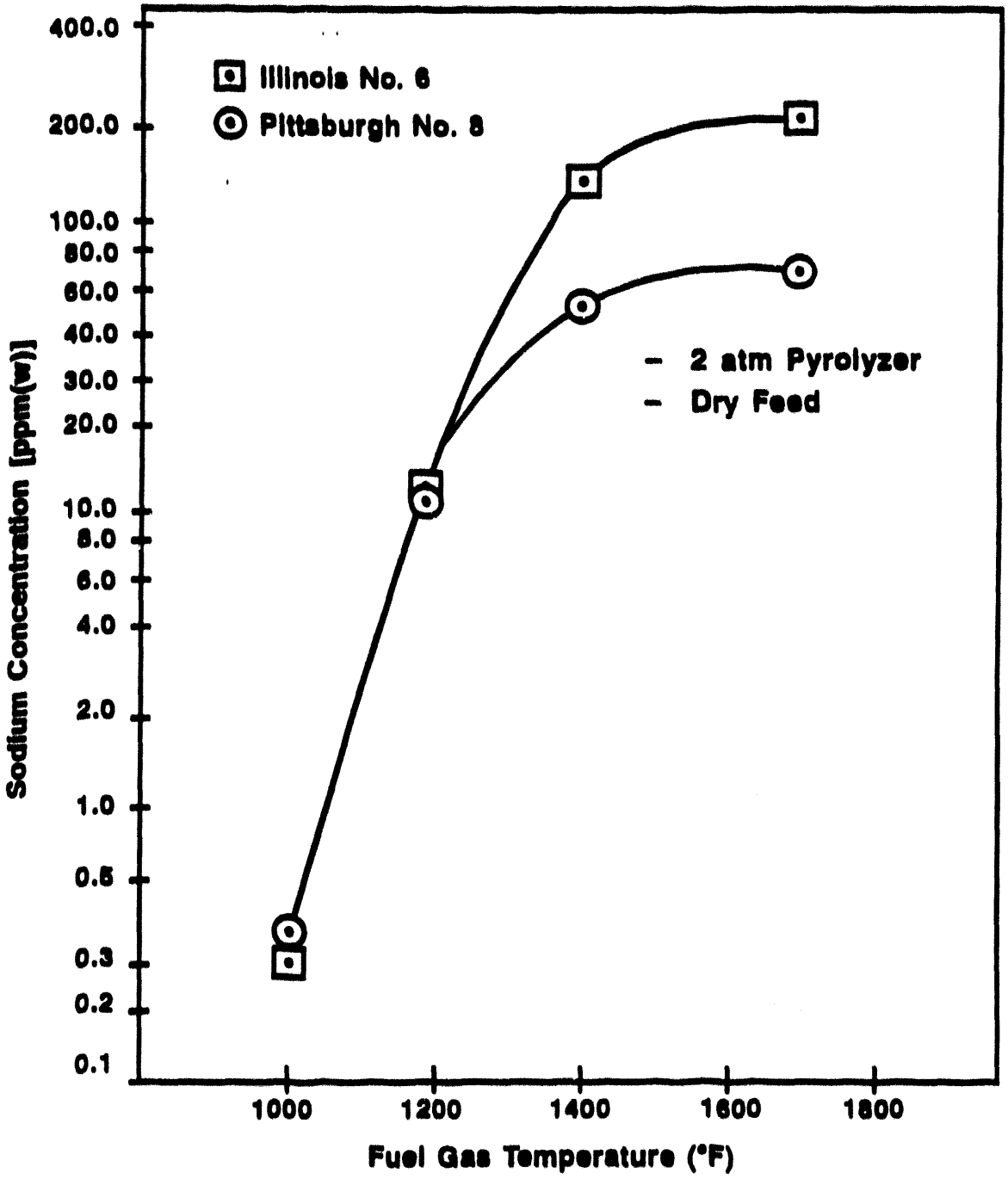

Figure 10 NG-HITAF—Fuel Gas Sodium Concentration vs. Temperature

Flat material specimens 1-in. wide by 2-in. long are being used in the test. The thickness of the specimens varies because of material availability. The Hexaloy SA specimens are 1/8-in. thick, the SiC_p/Al_2O_3 composite specimens are 1/4-in. thick, and the NT-230 specimens are 3/8-in. thick.

These tests are being run to evaluate the corrosive attack under conditions that approximate the conditions expected in the gas side of the ceramic air heater. The tests are being used to determine the relative resistance of the three materials to corrosion and generally determine the required level of fuel gas cleanup required. After exposure, the specimens are macroscopically and microscopically evaluated for material loss and effects of corrosion.

The specimens are loaded with ash that has been made from char/sorbent samples produced in the FWDC Second-Generation PFB pilot plant. The ash is applied to one side of each specimen. The amount of ash applied to specimens corresponds to the estimate of the loading that will accumulate in 100 hours. The specimens are then maintained at temperature in electric furnaces. An atmosphere of synthesized flue gas is maintained in the furnaces. The composition of the synthesized flue gas is shown in Table 5.

Table 5 Flue Gas Composition for Ceramic Corrosion Tests

Component	wt%
CO_2	18.54
H_2O	7.61
O_2	2.54
N_2	71.11
SO_2	0.0268

There are basically two types of corrosive environments that can exist in the ceramic air heater. One is in the gas inlet region where the maximum tube temperature will exist and any ash particles in the flue gas will generally be in a molten state. The other condition is towards the gas outlet where gaseous phase alkalies can condense and enhance the alkali level in the ash. The problem of alkali condensation can be eliminated by sufficiently cleaning the fuel gas of gaseous phase alkalies. The high-temperature corrosion can be eliminated by sufficiently removing particulates from the fuel gas. The purpose of these tests is to get a rough determination of the level of fuel gas cleaning that will be required. The test conditions run so far are listed in Table 6.

The deposits were applied to the specimens every 100 hours. The specimens lightly scraped to remove loose material and then the new deposit was added. The duration of the test runs was 500 hours.

Table 6 Ceramic Corrosion Test Conditions

Test Run	Temperature, °F	Specimens	Char/Sorbent*	Deposit Loading†, mg/in²	Deposit Composition, wt%			Test Duration, h
					Ash	$NaSO_4$	K_2SO_4	
1	2300	SiC-SA	Pittsburgh No. 8/Plum Run Dolomite Illinois No. 6/Longview Limestone Eagle Butte/Longview Limestone	23	100	0	0	500
2A	1800	SiC-SA SiC_p/Al_2O_3 Siliconized SiC	Pittsburgh No. 8/Plum Run Dolomite	600	56	42	2	500
2B	1800	SiC-SA SiC_p/Al_2O_3 Siliconized SiC	Pittsburgh No. 8/Plum Run Dolomite	600	93	6.6	0.4	500
3	2300	SiC-SA SiC_p/Al_2O_3 Siliconized SiC	Pittsburgh No. 8/Plum Run Dolomite Illinois No. 6/Longview Limestone Eagle Butte/Longview Limestone	600	100	0	0	500

*All combinations of ceramic type and deposit type are tested.
†Applied every 100 hours.

The results of Tests 1 and 2 are summarized in Table 7. Photomicrographs of the Test Run 1 specimens after exposure are shown in Figure 11. The conditions of this test run simulated the gas inlet region of the ceramic air heater with a barrier filter in the fuel-gas stream. With these relatively light ash loadings, no corrosion was evident with any of the three coal chars tested. At the time these tests were run, we only had a small furnace that was capable of 2300°F. For this reason, only the SiC-SA specimens were tested. We now have a larger furnace, and these test conditions will be repeated with all three materials.

Test Runs 2A and 2B were run simultaneously in the same furnace. These tests simulated the gas outlet region of the ceramic air heater where condensation of gaseous phase alkalies can increase the alkali concentration in the ash deposit. These tests were also run with higher ash loadings that could occur if a barrier filter was not used in the fuel-gas stream. Photomicrographs of these specimens are shown in Figures 12, 13, and 14. There was no corrosive attack on the SiC_p/Al_2O_3 even with the highest level of added sodium sulfate. There was attack on the other materials and the extent of this attack was greater with the higher level of alkali addition.

Subtask 3.10—Fuel Characterization Testing

During this quarter, fuel characterization testing at Brigham Young University (BYU) neared completion. Testing is being performed at BYU's Advanced Combustion Engineering Research Center (ACERC), with close cooperation between personnel at TRW and BYU. The overall objective of the testing is to obtain experimental data on high-temperature char reactivity and combustion characteristics in support of combustor analytical modeling and conceptual design activities.

Preliminary analysis of the char produced from FWDC's second-generation PFB combustion project indicates that, although the char contains only a fraction of the original coal volatiles, it still appears to be fairly reactive, apparently because of the conditions under which it is pyrolyzed.

Analyses and experiments are being performed at BYU to provide information on:

- Expected volatile yields at high heating rates (and comparison with ASTM tests)
- Char reaction rates as a function of particle residence time, gas temperature, and gas composition
- Preliminary information on nitrogen and sulfur release rates during char oxidation

Description of Experiments. The rates of char combustion, sulfur release, and nitrogen release are being determined in a flat-flame burner (FFB) experiment as a function of flame temperature, gas composition, and particle residence time. Both parent coal and char samples are being characterized. Gas temperatures and compositions have been selected to be similar to the actual slagging stage combustor environment (approximately 2000 K/3000°F). Since

Table 7 Summary of Test Runs 1 and 2 Results

Exposure Condition	2300°F for 500 h 23 mg/in² Ash Every 100 h			1800°F for 500 h 0.6 g/in² Ash					
	SiC-SA			SiC-SA		SiC_p/Al_2O_3		Siliconized SiC	
Ash	Pittsburgh No. 8	Eagle Butte	Illinois No. 6	Low Alkali Ash	High Alkali Ash	Low Alkali Ash	High Alkali Ash	Low Alkali Ash	High Alkali Ash
Material Interaction	No Significant Attack	No Significant Attack	No Significant Attack	Attack	Attack (More Severe Than Low Alkali)	No Significant Attack (Possible Material Microstructure Change Near Interface)	No Significant Attack (Possible Material Microstructure Change Near Interface)	Attack	Attack (More Severe Than Low Alkali)

- Low Alkali Ash: Pittsburgh No. 8 (92.7%), Sodium Sulfate (6.6%), Potassium Sulfate (0.4%)
- High Alkali Ash: Pittsburgh No. 8 (56.1%), Sodium Sulfate (41.7%), Potassium Sulfate (2.2%)

(A)

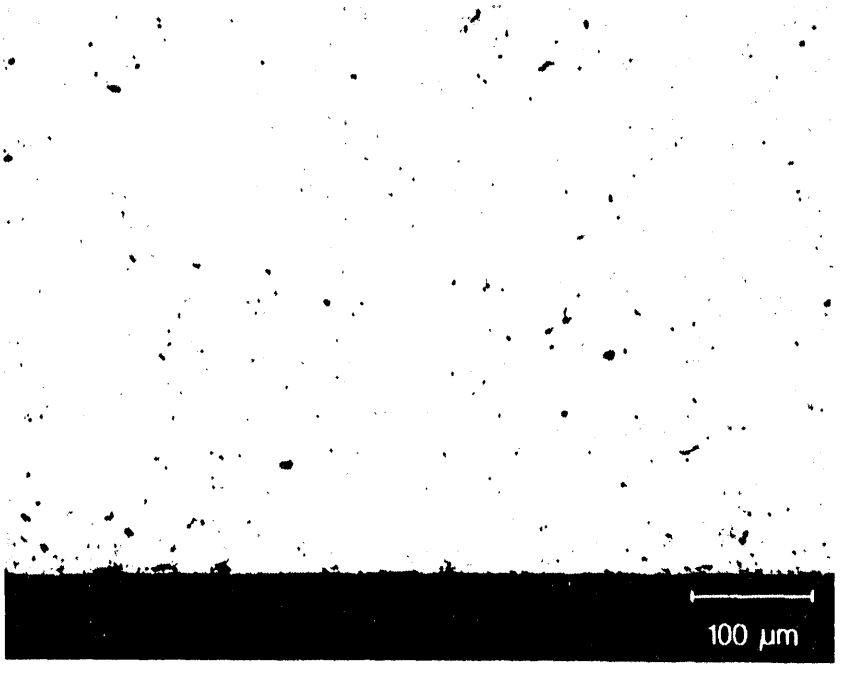

(B)

Figure 11 Micrographs of Polished Cross Section of Hexoloy Sample After Ash Exposure [(A) Ash deposit side (B) No deposit side]

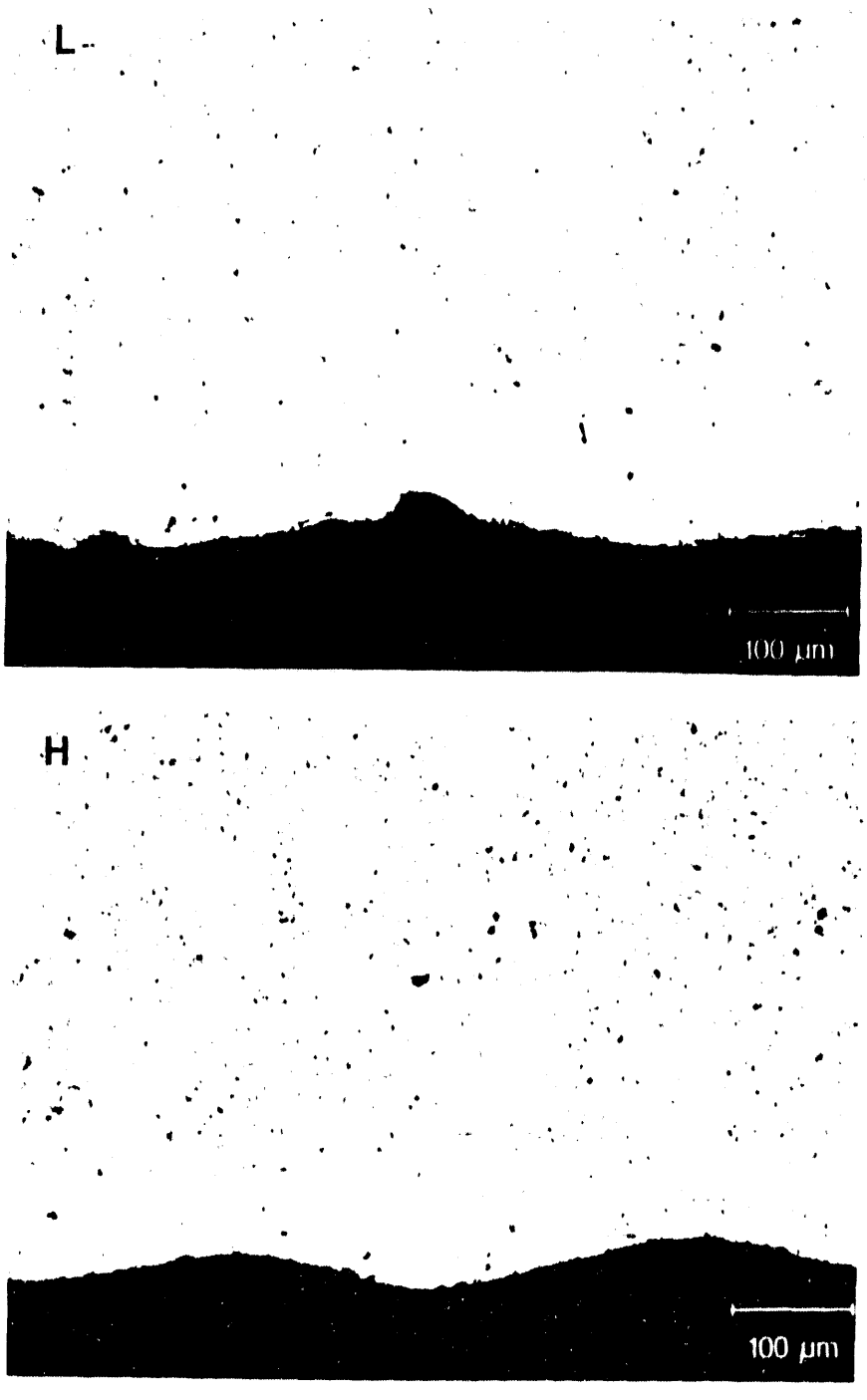

Figure 12 Micrographs of Cross Sections of Exposed Hexoloy Samples [(L) Low alkali ash (H) High alkali ash]

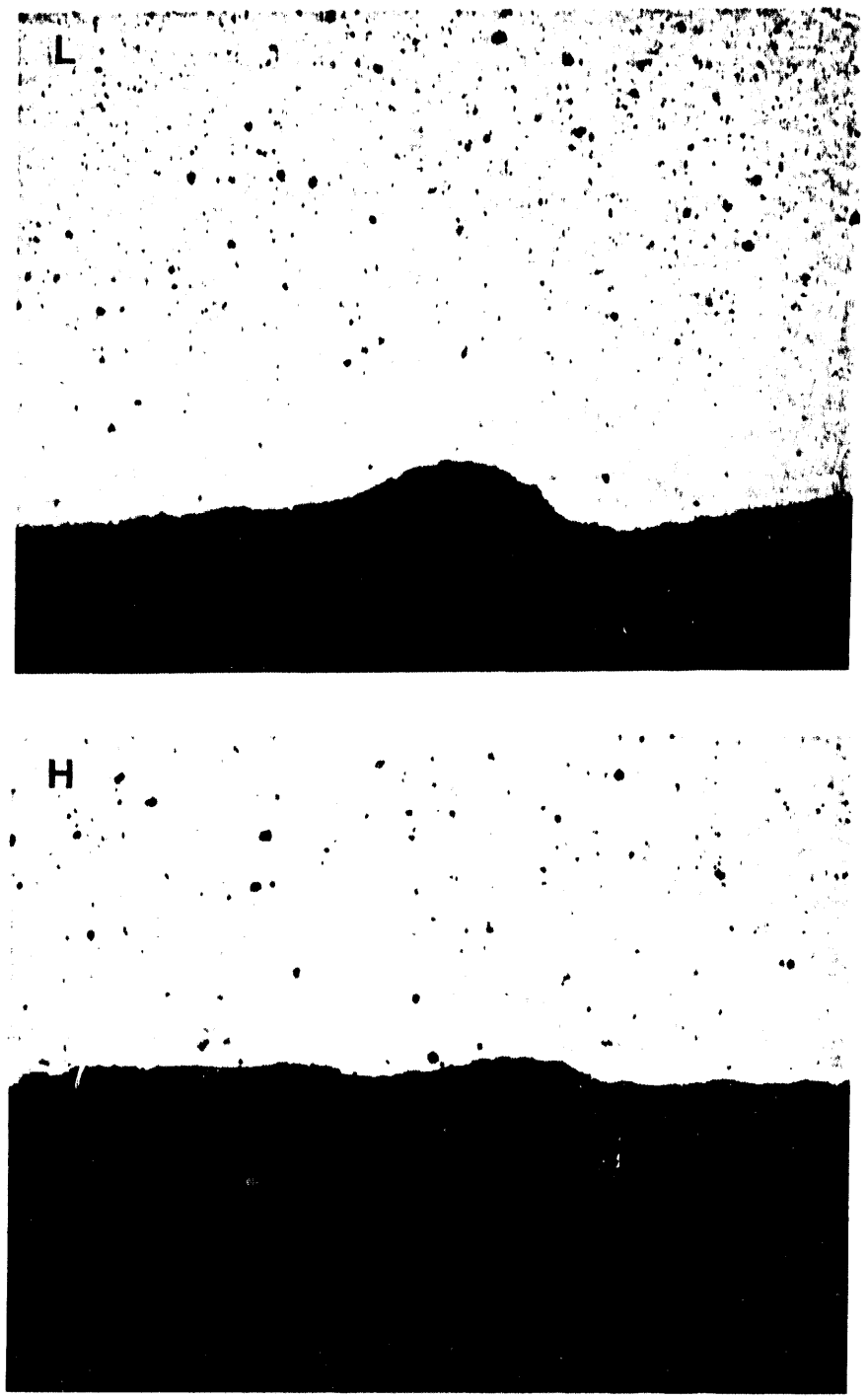

Figure 13 Micrographs of Cross Sections of Exposed Norton Samples
[(L) Low alkali ash (H) High alkali ash]

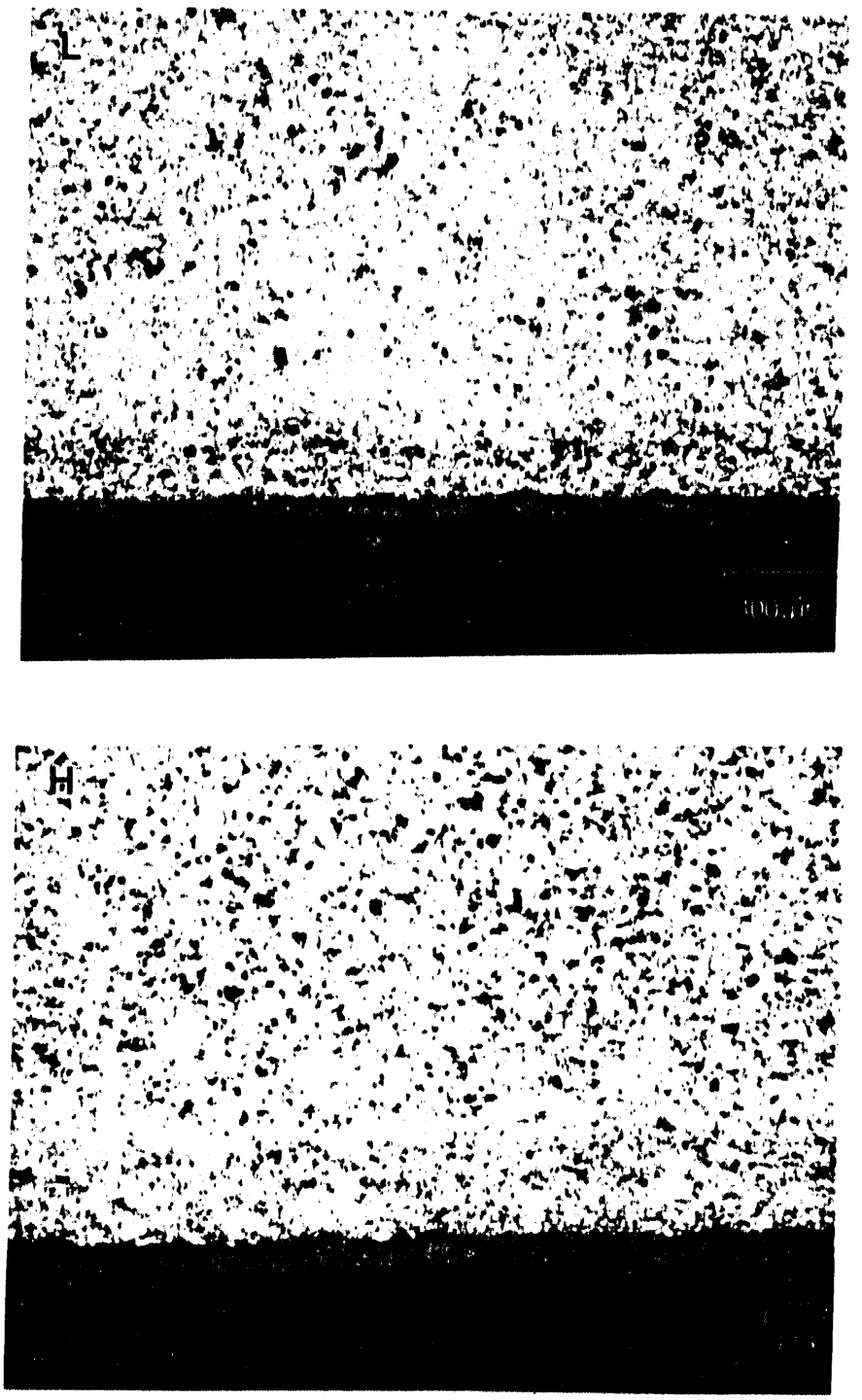

Figure 14 Micrographs of Cross Sections of Exposed Lanxide Samples
[(L) Low alkali ash (H) High alkali ash]

the slagging combustor design calls for complete conversion of the char particle in 70 to 90 percent of stoichiometric air, tests have been conducted in both oxygen environments and in steam/CO_2 environments.

The post-flame gases in the FFB experiment can be adjusted to contain 0 to 20 mole-percent O_2 by changing the stoichiometry of the flame. These post-flame gases generally contain 13 mole-percent steam and 6 mole-percent CO_2. Char samples are being collected in the FFB at different residence times in order to determine kinetic rates. Residence times in the FFB are being determined by streak photography. Maximum particle residence time in the FFB is approximately 500 ms, however, approximately only 80 ms is available for gas temperatures of interest.

A schematic of the FFB test configuration is shown in Figure 15. Air and methane are transported separately through a monolith structure, as shown in Figure 16. A steady, flat flame is produced at the top of the structure. Coal or char is fed pneumatically upwards through the middle of the FFB. An adjustable collection probe with a nitrogen quench is located above the FFB to collect and extinguish the burner char particles. The char is then collected by either a cyclone or filter for subsequent post-test analysis.

A series of modifications were performed to the sampling system during the course of the project. The original cyclone system was found to be inadequate for the proposed char, apparently because of the amount of fines generated during combustion. A glass fiber filer was also found to be inadequate because of retention of fines in the filter. The final sampling system for this project consisted of a 2.5-in. polycarbonate Nuclepore filter (1 micron pores) without the cyclone.

The particle residence time in the flame is controlled by varying the distance of the collection probe above the burner. The gas temperature is measured at various distances above the burner using Type B thermocouples inserted in the gas stream. The thermocouple reading is corrected for radiation losses through the transparent tower assuming the radiation losses balance the convective heat transfer to the thermocouple bead.

Post-test fuel analyses are being performed on collected char and compared with pre-test analyses to determine carbon, sulfur, and nitrogen loss. Results will be compared with those obtained with the parent coal. Analyses being performed on the parent coal and collected char samples include the following:

- Proximate analysis (ASTM volatiles, fixed carbon, moisture, and ash)
- Ultimate analysis (C,H,N,S; O by difference)
- Ti and Al tracer analysis (by ICP atomic adsorption spectroscopy)
- Apparent density (tap density technique)
- Internal surface area (N_2 and CO_2)

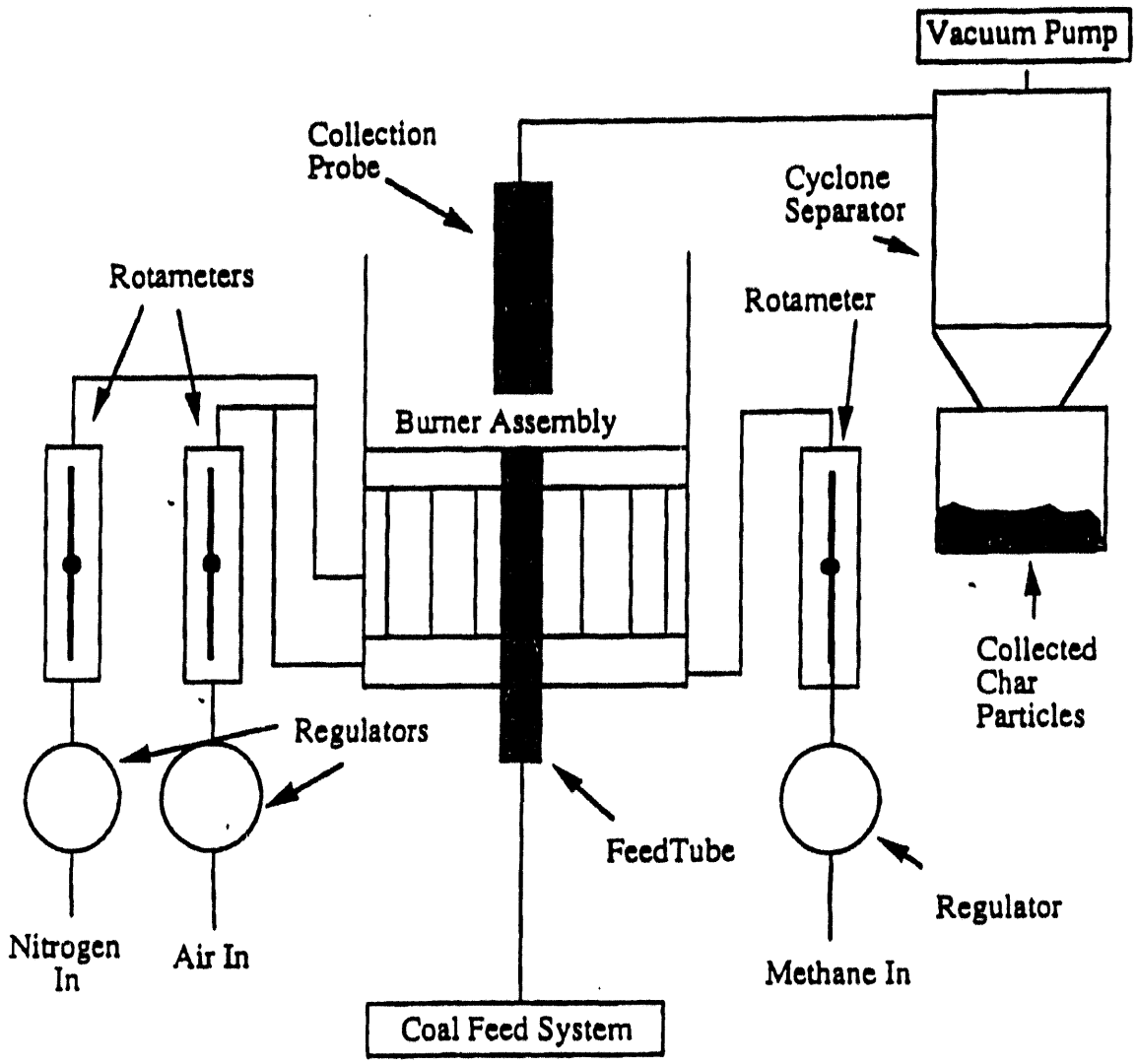

Figure 15 Schematic of the Flat-Flame Burner System

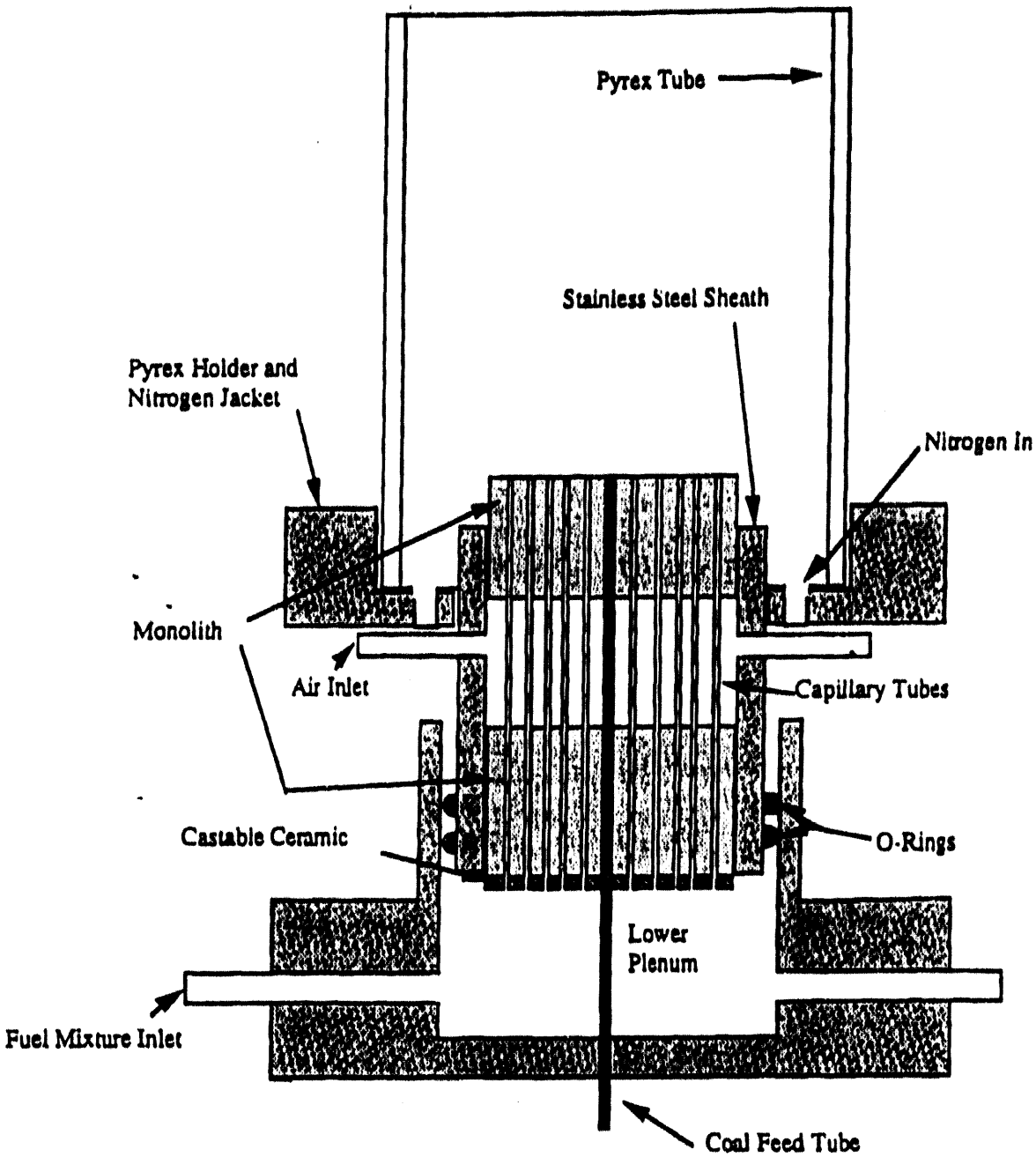

Figure 16 Schematic of the Flat-Flame Burner Assembly

Summary of Results. Results obtained to date include a characterization of both parent coal and char combustion in the baseline gas environment (1800 K, 5 percent O_2). Tests have also been performed for different gas temperatures and oxygen concentrations, however the results are still being analyzed and thus will be reported in the next quarterly report. Information is also available on changes in char surface area, apparent density, and chemical composition during burnout. This information is presented in the following sections.

Experimental Test Conditions. After several preliminary tests, three experimental conditions in the FFB were selected. Two of the conditions contained 5 mole-percent O_2 in the post-flame gases, and the third condition had 0 mole-percent O_2 in the post-flame gases. The measured gas temperature profiles for these conditions are shown in Figure 17. The decrease in gas temperature is due to convective heat losses from the reactor walls. The three conditions are referred to in this report as:

- 1800 K, 5-percent O_2
- 2000 K, 5-percent O_2
- 2200 K, 0-percent O_2

Particle velocities were measured using streak photography and compared with oscilloscope traces. The velocities were then integrated using a computer simulation of the burner, adjusting for temperature changes, and residence times were thereby determined. However, because of the high temperatures involved in these experiments, residence times for the different gas conditions changed by less than 5 percent at any location. This is probably the same accuracy as the residence time determination. Samples were taken at four distances from the top of the burner. The residence times for these locations are as follows:

Distance (in.)	Residence Time (ms)
0	0
2	20
4	40
6	60
8	80

Char Reactivity. Results of the coal and char reactivity and characterization tests for the baseline gas environment (1800 K, 5 percent O_2) are shown in Table 8. Burnout for individual samples were determined by an average of the values calculated from the titanium and aluminum tracers, using ICP atomic adsorption spectroscopy. Burnout results are reported on a dry-ash-free (DAF) basis.

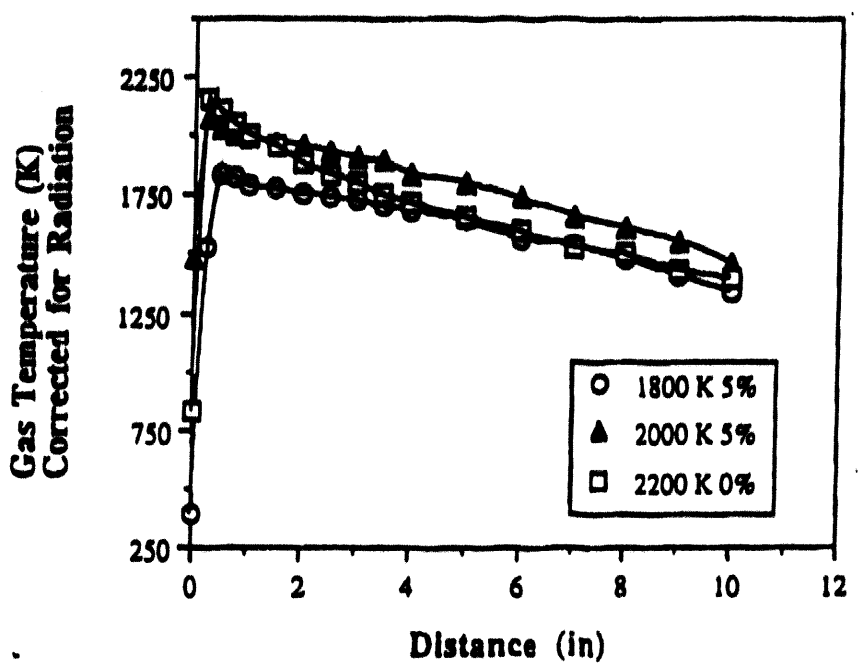

Figure 17 Gas Temperature Profiles of Three Gas Conditions Used for Char Combustion Experiments

Table 8 Char Burnout Results (1800 K, 5-Percent O_2)

Fuel	Sampling Distance, in.	Average Burnout, % DAF		Average Apparent Density, g/cm^3	N_2 Surface Area, m^2/g	CO_2 Surface Area, m^2/g
		Including Volatiles	Char Only			
Pittsburgh No. 8 Coal	2	50.4	0	0.38	77	241
Pittsburgh No. 8 Coal	4	58.6	14.1	0.37	44	241
Pittsburgh No. 8 Coal	6	60.5	29.6	0.42	37	188
Pittsburgh No. 8 Coal	8	63.5	30.3	0.47	33	134
Pittsburgh No. 8 Char	2	N/A	10.6	0.70	31	146
Pittsburgh No. 8 Char	4	N/A	20.4	0.65	28	149
Pittsburgh No. 8 Char	6	N/A	29.2	0.67	33	135
Pittsburgh No. 8 Char	8	N/A	34.7	0.68	31	101

In order to compare the post-volatile char burnout rates for both the parent coal and char, the coal data was corrected to account for devolatilization. The corrected coal burnout data is also listed in Table 8. The value of the coal burnout at the first sampling position (2 in.) is taken as the volatile yield for the coal. This is approximately the location in which the intensity of the individual burning coal particles was observed to decrease significantly, indicating a transition between devolatilization and char oxidation.

Char burnout for both the coal and char as a function of sampling distance above the flat flame burner is compared in Figure 18. In addition, the burnout for the 63- to 75-mm size fraction of a Pittsburgh No. 8 coal from the DOE/PETC data base (the same coal used by Hurt and Mitchell [12]) is shown for the 1800 K, 5 mole-percent O_2 condition. Important conclusions from the data are as follows:

- The char burnout for the Pittsburgh No. 8 char, which was obtained from the FWDC Second-Generation PFB pilot plant occurs at a slightly greater rate than the char burnout of the parent coal, after accounting for devolatilization.

- The char burnout for the Sandia Pittsburgh No. 8 coal, normalized for volatile yield, is slightly lower in the 1800 K/5-percent O_2 environment than the burnout for the FWDC Pittsburgh No. 8 coal or 330 char.

Char Properties. Physical properties of the respective coal chars were measured in order to better compare char reactivities with known data. Apparent densities and internal surface areas were measured and compared with char property data from other experiments. A summary of results from this project is found in Table 8. The surface areas of coals and chars from other projects are listed in Table 9, and compared with chars from this project in Figures 19 and 20. Figure 19 shows that the parent coal exhibits properties similar to those reported for other coals of similar rank (percentage of oxygen in the DAF coal is used as a rank indicator). Figure 20 shows that the surface areas of the parent 330 char and of the partially-reacted chars from both the coal and the 330 char are similar to surface areas of other chars prepared in FFB's.

The apparent densities of the coal and char during burnout are also given in Table 8, and are shown in Figure 21. These values represent averages from several experiments. A packing factor of 0.6 g/cm^3 solid/tube was used to derive the values of the apparent density, which allows the parent coal to have an apparent density of 1.3 g/cm^3. As the coal devolatilizes, the char reaches a density of about 0.4 g/cm^3 and then slightly increases to about 0.47 during char combustion. The 330 char increases in apparent density during devolatilization from 0.5 g/cm^3 to approximately 0.7, and then remains at 0.65 to 0.70 g/cm^3 during char oxidation. As a comparison, the Pittsburgh No. 8 char studied at Sandia had an initial apparent density of 0.4 g/cm^3, and the apparent densities of chars of other coals ranged from 0.26 to 0.68 [2]. The slight densification of the 330 char during high temperature devolatilization is not uncommon, especially when the char is generated at low to moderate temperatures [14].

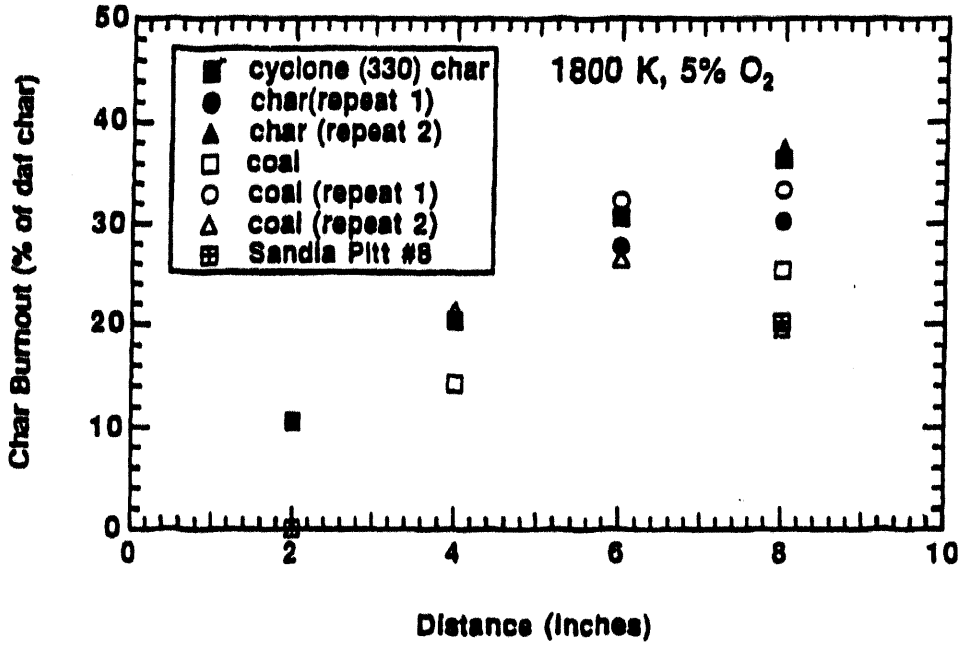

Figure 18 Char Burnout vs. Distance in the Flat-Flame Burner for the 330 Char and the Parent Pittsburgh No. 8 Coal in the 1800 K, 5 mol% O_2 Environment. [Burnouts are the averages of the values calculated from the Ti and Al tracers. Char burnout for a Pittsburgh No. 8 coal (PSOC 1451, 63-75 μm size fraction) is also shown.]

Table 9 Coal and Char Surface Areas From Other Experiments

Description	Coal	Coal N_2	Char N_2	Coal CO_2	Char CO_2	%C Coal (DAF)	%O Coal (DAF)
Cope (1992)	Dietz (subb)		229		337	72.9	17.3
			65			72.9	17.3
	Zap (lig)		190		543	76.0	20.3
Hyde (1990)	Pitt No. 8 (hvab)		85		214	83.3	6.8
	Dietz (subb)		217		301	72.9	17.3
	Zap (lig)		140		301	76.0	20.3
White (1989)	Zap (lig)	0.5		242	476	76.0	20.3
		1		268		76.0	20.3
		1.9		238		76.0	20.3
				115		76.0	20.3
	Wyodak (subb)	5		207		75.0	18.0
		2.6		308		75.0	18.0
	Pitt No. 8 (hvab)	1.3	93	118	252	83.2	8.8
		1		141		83.2	8.8
	Poc (lv)	1		231		91.1	2.5
		2.8				91.1	2.5
	Wilcox (lig)		47		252	72.3	20.1
			124			72.3	20.1
Hurt, et al. (1992)	Hiawatha (hvcb)	1	135	140	325	79.6	13.3
			120		410	79.6	13.3
	Lower Kit (lvb)	1	5	110	400	88.2	3.5
			60		280	88.2	3.5
TRW (This project)	Pitt No. 8 Coal	1.3	77	138	241	79.0	10.5
	330 Char	103	74	279	220	79.0	10.5

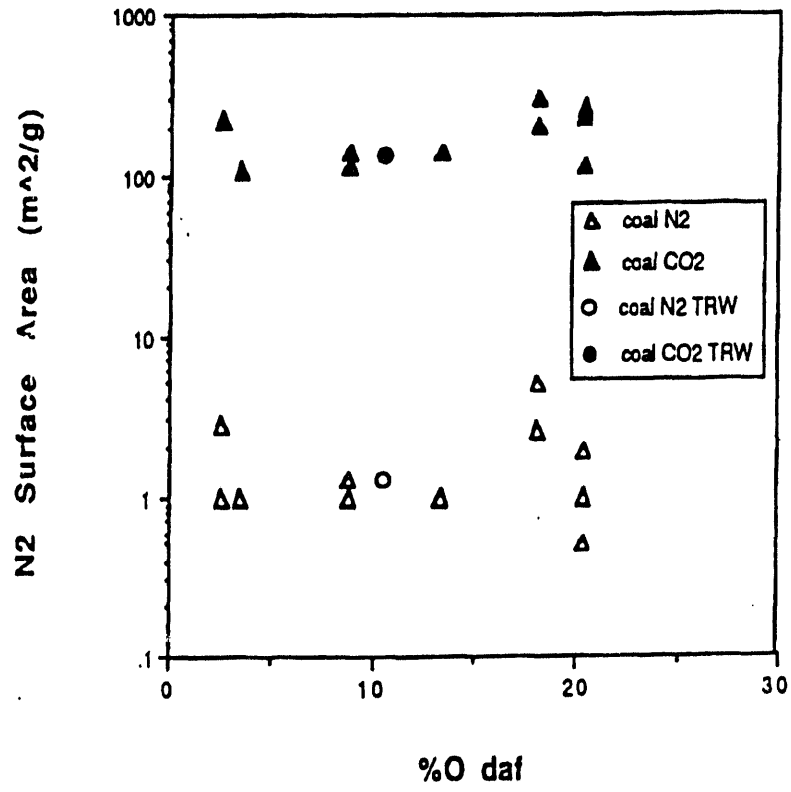

Figure 19 **N_2 and CO_2 Internal Surface Areas of the Parent Pittsburgh No. 8 Coal Used in This Project Compared With Literature Values for Other Coals. (The percentage of oxygen in the DAF parent coal is used as an indicator of rank, and the logarithmic scale is used to show the N_2 and CO_2 surface areas on the same graph.)**

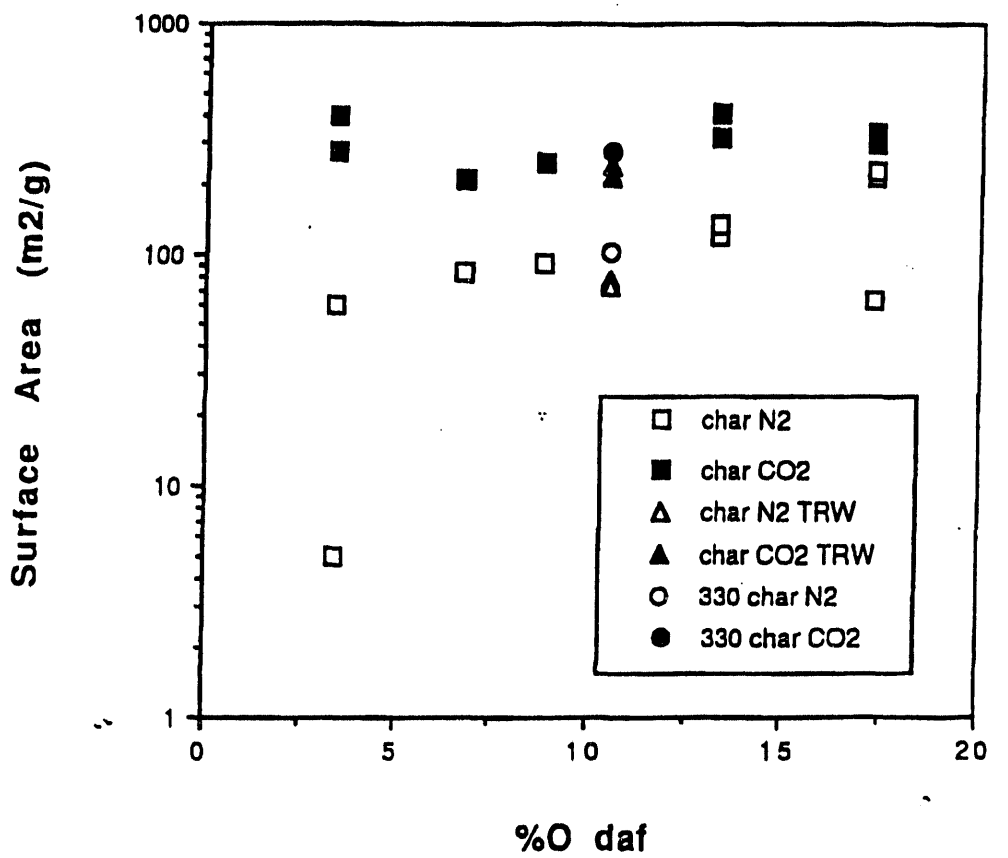

Figure 20 N_2 and CO_2 Internal Surface Areas of the Chars Used in This Project Compared With Literature Values for Other Chars Immediately After Devolatilization. (The percentage of oxygen in the DAF parent coal is used as an indicator of rank, and the logarithimic scale is used to shown the N_2 and CO_2 surface areas on the same graph.)

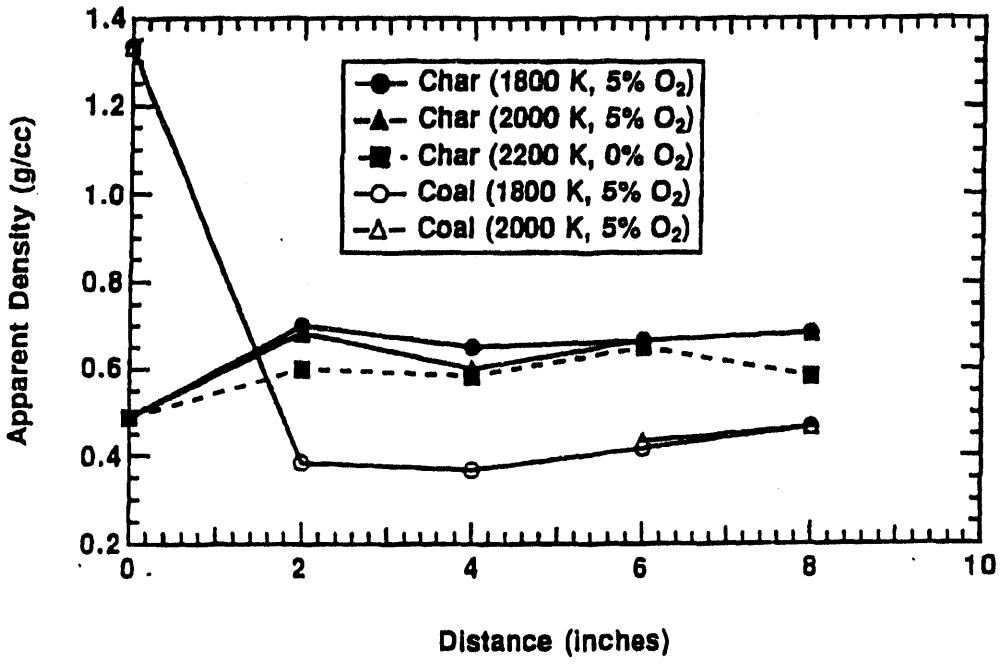

Figure 21 Apparent Densities of Coal and Char Samples From the Flat-Flame Burner Experiments

Hydrogen, Nitrogen and Sulfur Release. Preliminary information on the release rates of hydrogen, nitrogen, and sulfur is available for both coal and char samples in the 1800 K/5-percent O_2 flame environment, and are summarized in Table 10. Results are compared after 80 ms of exposure in the high-temperature FFB environment. The results have been normalized to the rates of carbon consumption. For example, a value of 1.34 for the sulfur release rate in Column 1 of Table 10 indicates that sulfur is released at 1.34 times the average rate of carbon consumption during the 80 ms of exposure.

The coal data in Column 1 indicates that hydrogen is consumed at a rate much greater than carbon, which is expected since most of the coal hydrogen is known to evolve during devolatilization. On the other hand, sulfur and nitrogen are released at a rate of 1.3 to 1.4 times the carbon burnout rate.

For the char, which includes spent sorbent primarily in the form of CaS, the sulfur release rate is still greater than the rate of carbon consumption, indicating that most of the sulfur contained within either the coal or spent sorbent is likely to be released during char oxidation at high temperatures. The nitrogen release rate appears to be comparable to the carbon consumption rate, while the hydrogen consumption rate is lower than the carbon rate. This last result is not surprising, since such a small fraction (approximately 4 percent) of the coal hydrogen remains in the char following pyrolysis.

Preliminary Conclusions From Fuel Characterization Testing. Although all the data from the fuel characterization tests conducted at BYU has not been completely analyzed at this time, the following preliminary conclusions can be drawn based on the data obtained to date:

- The char burnout rates for Pittsburgh No. 8 coal and FWDC char under high-temperature, oxygen rich conditions are comparable. Hence, in addition to the information obtained during BYU testing, kinetic rate data obtained from other studies of Pittsburgh No. 8 coal can be used for analytical modeling of post-devolatilization char burnout. This includes the comprehensive set of apparent reactivities for high-temperature char oxidation recently published [12].

- Measured char surface area and apparent densities at various stages of burnout are within the range of values measured in other kinetic studies. This further validates the approach of using previously determined kinetic parameters for modeling the burnout of the FWDC char.

- The sulfur contained within the char and spent sorbent mixed was determined to be released at a rate at least as great or greater than the observed char burnout rate under high-temperature conditions. Hence, it is expected that most, if not all of the sulfur introduced into a high-temperature flame zone will be gasified during char oxidation.

Table 10 Comparison of Sulfur, Nitrogen, and Hydrogen Consumption Rates in Flat-Flame Burner*

Fuel	Pittsburgh No. 8 Coal	Pittsburgh No. 8 Char
Flame Temperature, K	1800	1800
Oxygen Concentration, %	5	5
Residence time, ms	80	80
Consumption Rates:		
Sulfur	1.34	1.46
Hydrogen	5.03	0.74
Nitrogen	1.31	0.93
Carbon	1.0	1.0

*All sulfur, nitrogen, and hydrogen release rates are normalized to carbon burnout rate.

Subtask 3.18—Ceramic Air Heater Thermal/Structural Analysis

The ceramic air module is shown in Figure 22. Four of these modules are required for a 290-MW plan. The ceramic air heater modules are made up of multiple header/tube modules. The header/tube modules can be seen in Figure 22 and one header/tube module is shown in more detail in Figure 23.

One of the key structural concerns for the ceramic air heater is the generation of thermal stresses caused by differential thermal expansion between tubes joined to the same manifold. Tubes at different average temperature will expand to different lengths, resulting in stress loading at tube-to-manifold junctions. The stresses will be distributed between the tubes and the inlet and outlet manifolds.

Each header/tube module has three rows of tubes in the gas-flow direction and 20 rows of tubes in the no-flow direction. The normal heat transfer process results in tubes in the gas-flow direction being at different temperatures. If uniform air and gas flow is assumed in the no-flow direction, the no-flow tubes should be at the same temperature. This has been assumed for the initial analysis. Subsequent analysis will consider the effects of no-flow direction flow maldistribution.

To determine the resulting stresses, a finite-element model of a complete module was prepared, using ANSYS Version 5.0, a commercially available structural and thermal analysis computer code. The model, which comprises approximately 1800 nodes, is shown in Figure 24. The substantial stiffening effects of the tube internal cruciform fins are included. The inputs to the model include the steady-state tube temperature distributions derived from the Aerospace Systems and Equipment inhouse heat exchanger performance analysis computer program. The temperature distributions include the contribution of radiation effects between tubes. At present, radiation effects to the first row of tubes from the heat exchanger sidewalls or the radiating gas mass in the gas duct are not included.

The average tube temperatures for the three rows of tubes in the first module (in the gas-flow direction) are 1960, 1999, and 2041°F. This is the hottest module, and exhibits the largest tube-to-tube temperature difference. The temperature variation along each tube is around 340°F. However, it is the average temperature difference that is the primary contributor to thermal stresses. Other inputs to the structural model include the internal pressure load (200 psi) and the self-weight load (tubes assumed to be in the horizontal plane). The manifold boundary conditions include spring mounting (metallic bellows) and typical values for sliding friction in the supports.

The predicted stresses are shown in Figure 25. The maximum principal tensile stresses are shown. Maximum principal stresses are generally used for ceramic structural analysis rather than von Mises stresses since ceramics are much stronger under compression than tension. The peak predicted maximum principal stress is around 21.0 ksi. As shown in the expanded view presented in Figure 26, the peak stresses exist in the manifold, at the tube-to-manifold junction. The peak stress components are summarized in Table 11 for both the tube side and manifold side of the junction.

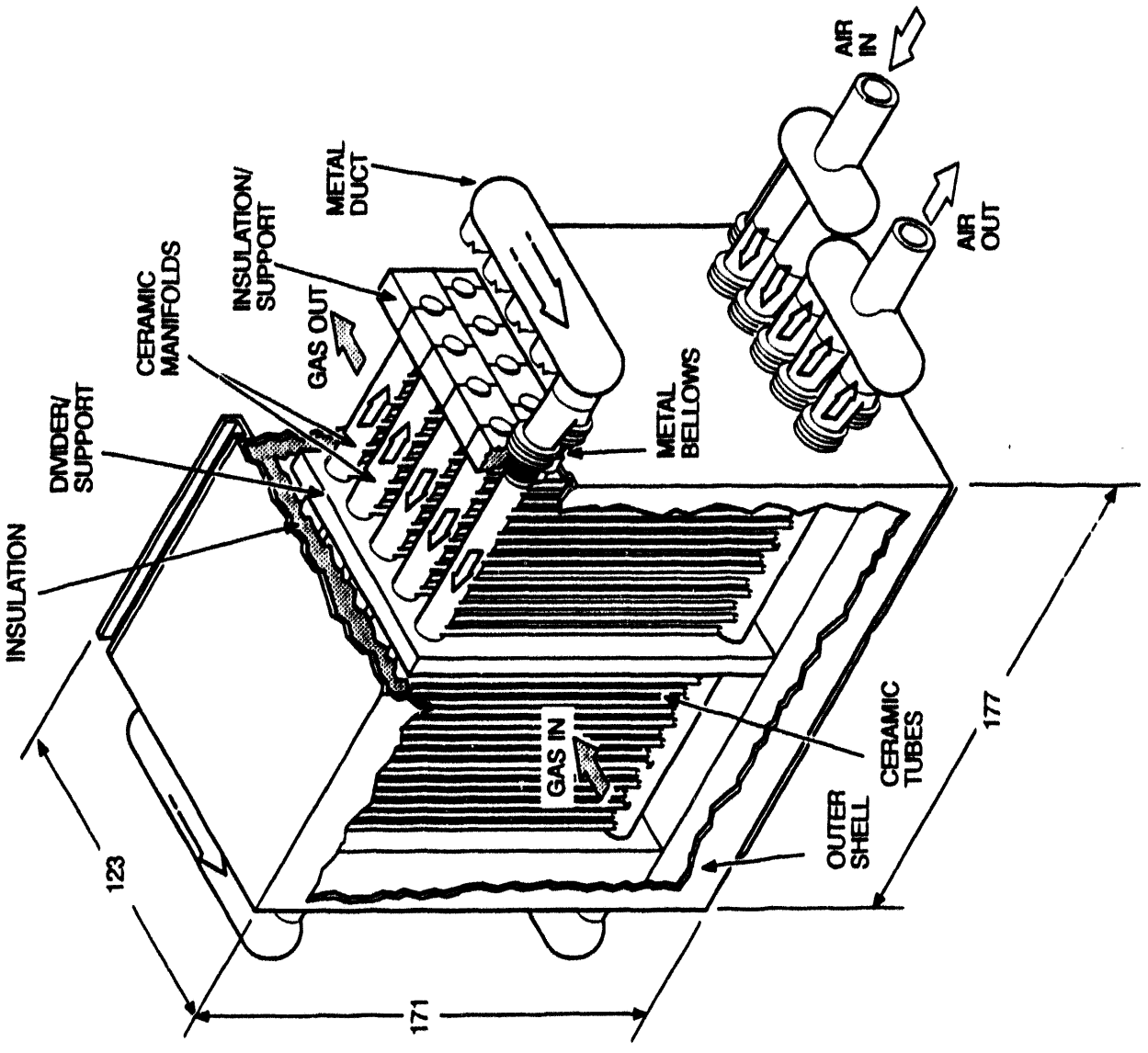

Figure 22 Ceramic Air Heater Module

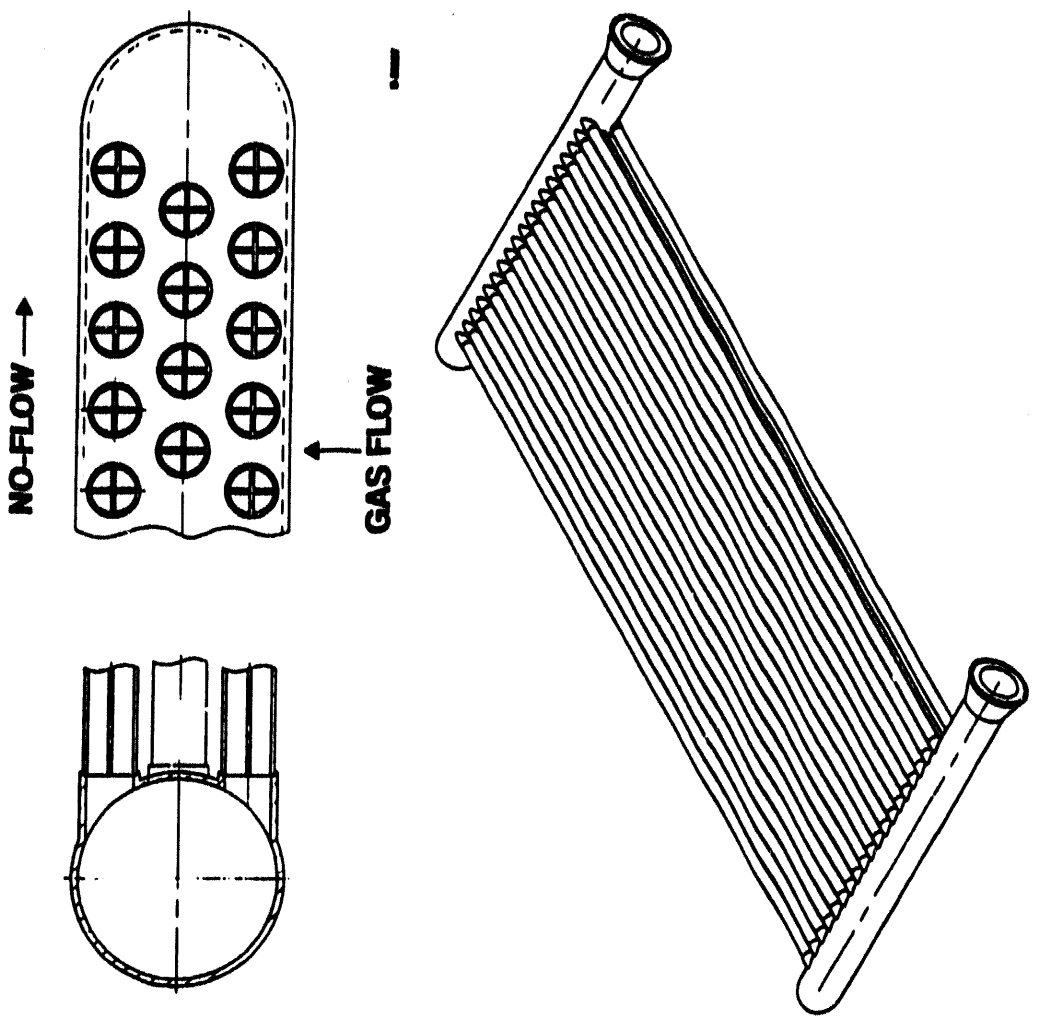

Figure 23 Header/Tube Module

1781 nodes
1838 elements

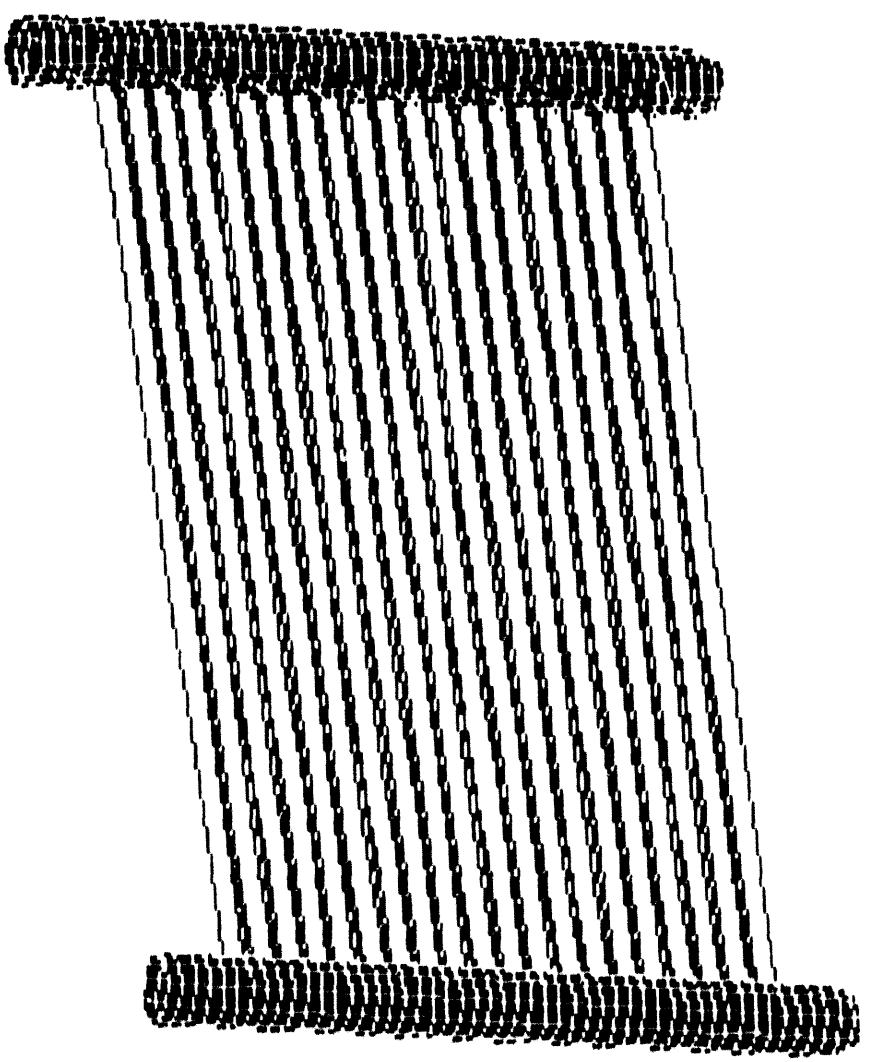

Figure 24 Header/Tube Model Coarse Grid

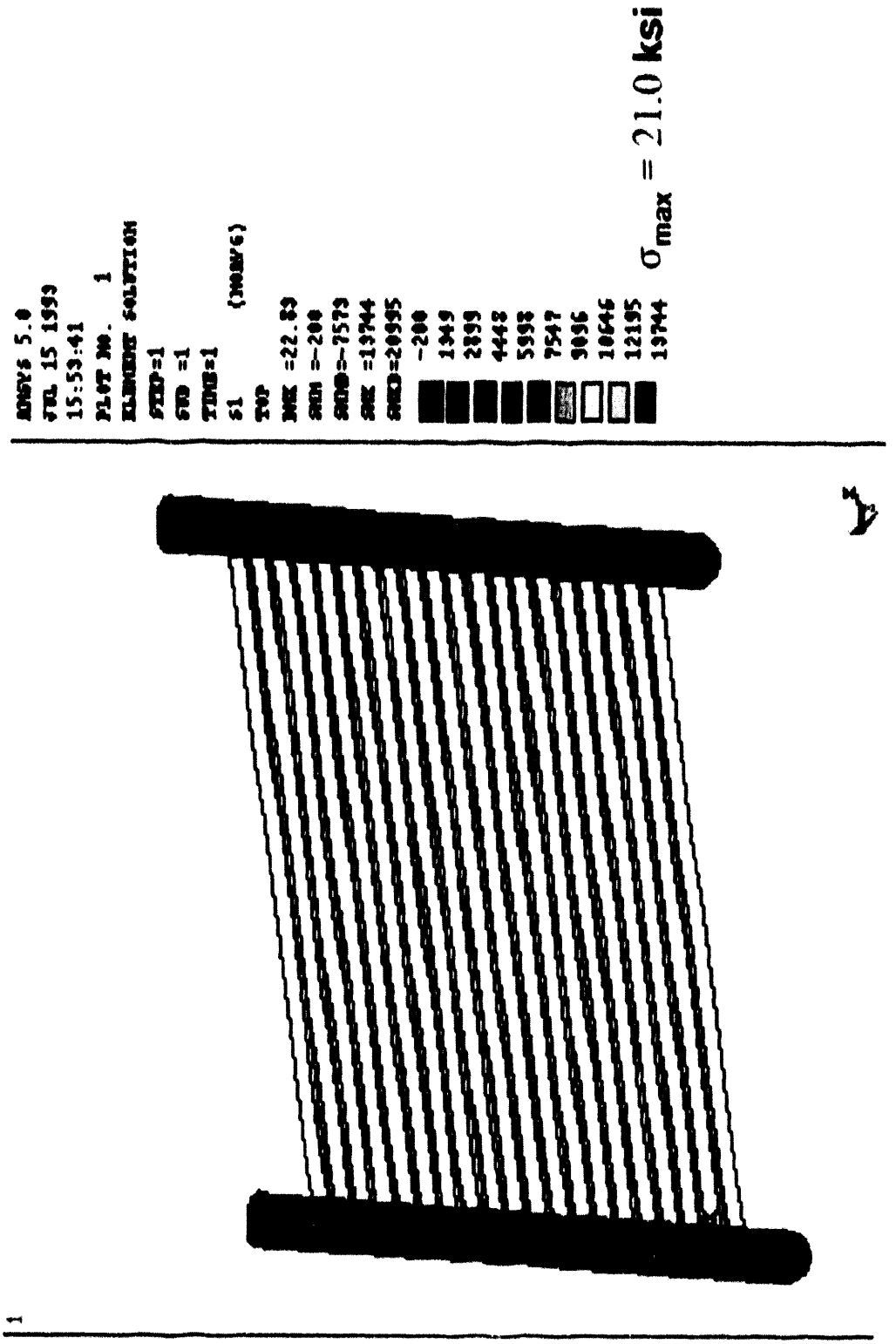

Figure 25 Maximum Principal Tensile Stress Plot

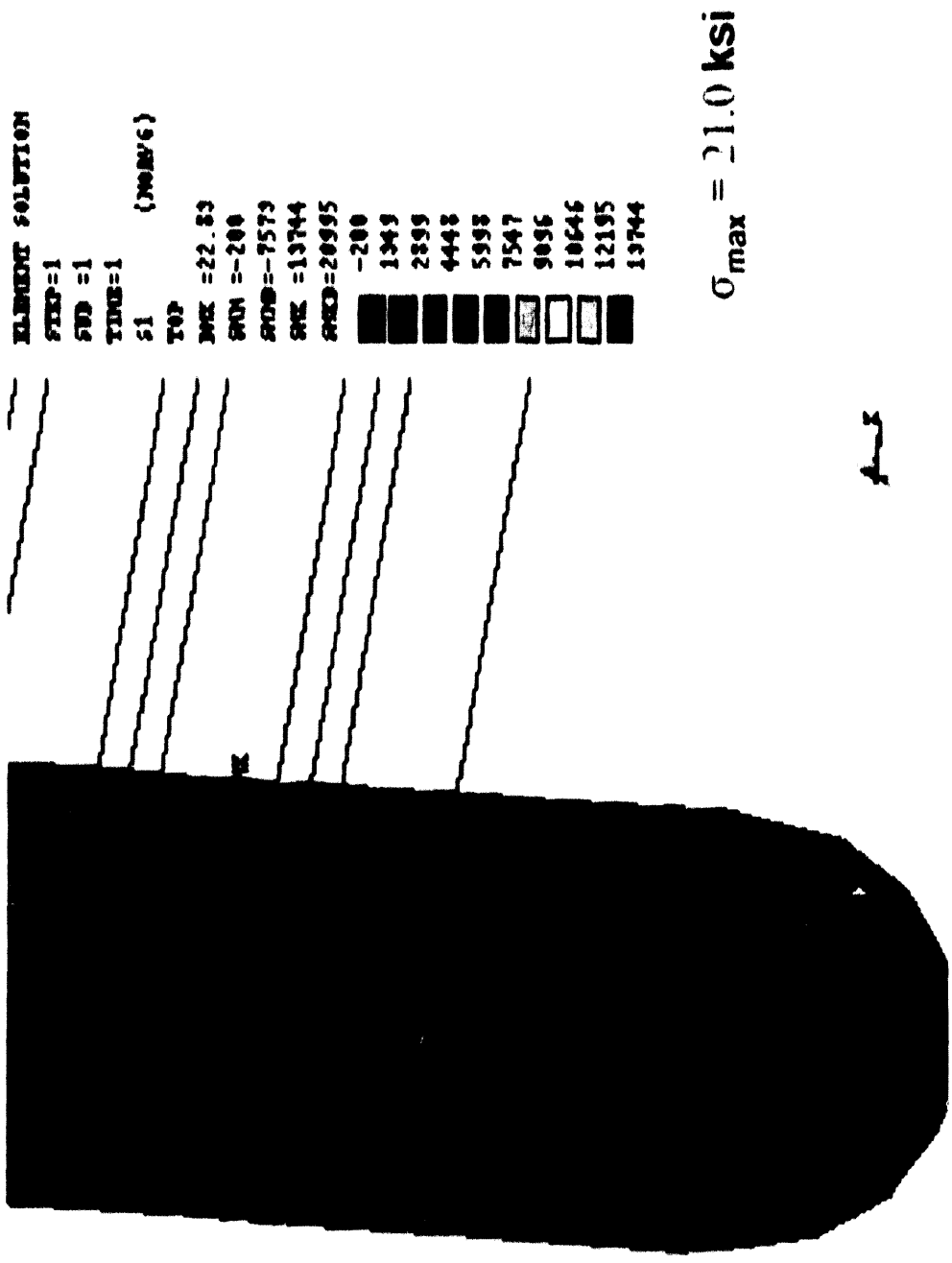

Figure 26 Expanded Maximum Principal Tensile Stress Plot

Table 11 Peak Stress Summary

Load Type	Manifold Stress, ksi	Tube Stress, ksi
Pressure	4.2	0.7
Weight	2.1	0.3
Thermal	19.3	2.4
Combined	21.0	2.8

The results shown in Table 11 indicate that the pressure and self-weight loads are low. In addition, the tube thermal stresses (because of axial expansion) are also low. The key stresses are the thermal stresses in the manifold at the tube junction.

Typical characteristic strengths for the baseline material, sintered alpha-silicon carbide, are in the 40 to 50 ksi range at operating temperatures. Life predictions for structural ceramics generally require a statistical analysis approach. For reasonable survival probability, the peak stress must be low with respect to the characteristic strength. The predicted peak stress of 21 ksi compares favorably with typical characteristic strengths. A favorable situation resulting from the stress fields (see Figure 26) is the highly localized nature of the peak stress. This results in a higher probability of survival compared to a broader stress field at the same peak value.

To enhance the precision of the stress predictions, a fine grid ANSYS model was prepared at the tube-to-manifold junction. This grid is shown in Figure 27. Loads and displacements resulting from the overall module model will be input to the finer grid model. The procedure will enable prediction of any stress concentration effects because of geometric changes at the junction.

If use of the fine grid model and the statistical analysis result in an unacceptably low probability of survival, it is likely that the stresses can be reduced. Because of much higher manifold stresses compared to tube stresses (see Table 11), a possible approach for peak stress reduction is to decrease the tube stiffness relative to the manifold stiffness. This should increase the tube stress while decreasing the manifold stress. The stiffness change might be effect by decreasing the cruciform fin thickness, decreasing the tube wall thickness, or increasing the manifold wall thickness.

Subtask 3.21—Pollution Control Systems

During this quarter, the SO_2, NO_x, and particulate material balances were recalculated. This was done to incorporate the latest plan heat and material balance (4/14/93) and to incorporate some changes in NO_x inputs. The systems emission model has been described in previous Quarterly Reports [15].

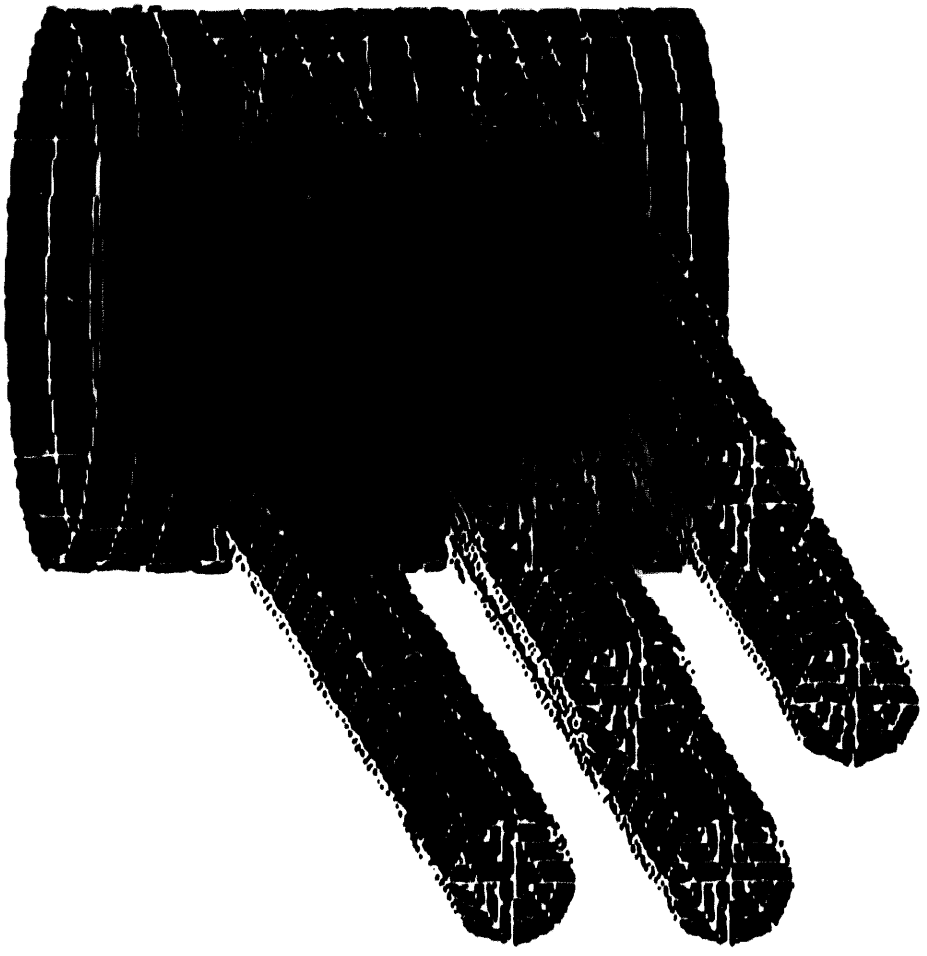

Figure 27 Fine Grid For Model

Previous estimates of NO_x from the fuel gas combustion were based on in house experience with low temperature fuel gas and combustion air. An investigation of the literature and requests to several burner manufacturers did not turn up any information on the NO_x production with low-Btu fuel gas and air at elevated temperatures. There has been some research done on the combustion of natural gas with preheated combustion air [16]. This research indicates that there is significant increase in NO_x production as air preheat temperature is increased when firing natural gas. This trend should also be present when firing low-Btu fuel gas, but we have not been able to find any data.

Fuel gas burner tests will probably be included as part of the Phase 2 proposal. Until we get better data we have used data from reference 16 and have used 260 ppm as the NO_x level for 1000°F vitiated combustion air. This level of NO_x production will require a backend $DeNO_x$ system. A 50-percent efficient SNCR system was added. The results are shown in Table 12, where it can be seen that 0.1335 lb/mm Btu is the system NO_x emission rate.

Because of the present uncertainties in levels of NO_x generation, a sensitivity study was done to determine the increases in NO_x production that could be tolerated while still meeting the goal of 0.15 lb/mm Btu emission. The result of this study is shown in Figure 28. The dark horizontal line represents the base case analysis shown in Table 12. If any one NO_x source is increased while the remaining two are held constant, one can proceed along that source line up to the limit of 0.15 lb/mm Btu system emission. The difference on the horizontal axis is then the increase in NO_x generation that can be tolerated. It can be seen that about 50 percent increase in any one of the inputs is possible. This allowance is reduced considerably if multiple generators increase NO_x production. Uncertainty in the gas turbine and char combustor NO_x emission will be reduced when the Phase 1 testing is completed.

Four candidate sulfur removal systems have been selected for possible use in the HIPPS plant. These are the Tung, SOXAL, CANSOLV, and Dow processes. These processes were discussed in Quarterly Report 4 [17]. The Tung process is being used in the current plant heat and material balances. The Tung system pilot unit will begin testing shortly at Niagra Mohawk Dunkirk Station. The SOXAL system testing at the same plant has been completed. Dow Chemical has elected not to pursue the development of its amine scrubbing regenerable system, but the Union Carbide CANSOLV system will be tested at Alcoa.

Subtask 3.27—Char Combustor Analytical Modeling

General Approach. Several different levels of analytical modeling are being performed in support of char combustor conceptual design. Key questions that are being addressed include:

- What are the residence time requirements necessary to achieve near complete burnout of the char (greater than 99 percent)?
- What precombustor preheat temperature is required to ensure adequate flame stability within the head end of the combustor?

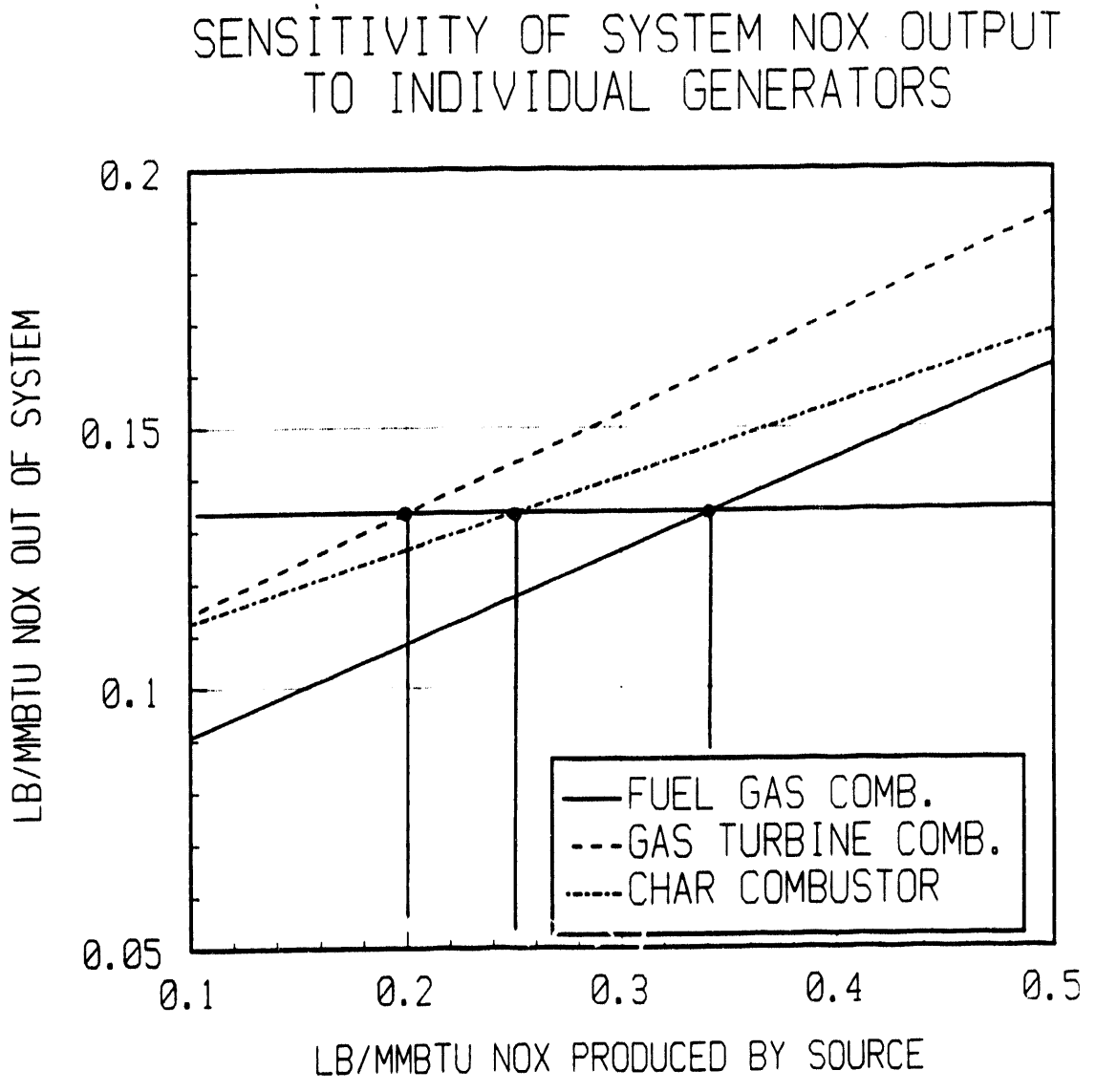

Figure 28 NO_x Source Sensitivity

- What char particle size distribution is required for both subscale and full scale combustor operation? How sensitive is combustor performance to char particle size variations?
- What NO_x emissions are expected? What combustor design and operational changes can be implemented to ensure that program NO_x goals are met?
- What is the expected combustor heat load to the cooling water circuit?
- What is the expected slag recovery? How sensitive is slag recovery to particle size variations?
- What is the combustor operating envelope as defined by carbon burnout, cooling load, pressure drop, NO_x emission, and fouling considerations?

The approach to answering these and other questions is as follows:

- A one-dimensional char oxidation model is being used to determine approximate residence time requirements as well as the effect of particle size variations on char burnout.
- A multi-zone combustor model is being used to address flame stability, char burnout, and NO_x formation. Key parameters that are being investigated are the effect of stoichiometry, precombustor preheat, injector and combustor geometry, and char particle size.
- A coal combustor engineering model is being used to determine combustor pressure drop, heat fluxes, cooling loads, slag flow, and slag recovery, for a given combustor geometry. Results from char oxidation modeling are used as inputs for this model.

Preliminary char oxidation calculations have been performed using kinetic parameters based on studies with Pittsburgh No. 8 coal in high-temperature environment [12] and are discussed in the following section. Detailed calculations with the multi-zone combustor model are now being performed based on the information obtained from BYU fuel characterization testing. Once this activity is completed, coal combustor engineering model calculations will be performed in order to finalize char combustor conceptual design and operating conditions. These models are proprietary; however, non-proprietary descriptions of the models will be prepared for the next quarterly report.

Preliminary Calculations. Preliminary char oxidation calculations were performed to determine the approximate residence time requirements for the char combustor, as well as to determine the effect of particle size on char burnout. The purpose of these calculations were to help determine the approximate scale of testing during Phase 2 of the HIPPS program, as well as to estimate the particle size range required during both sub-scale and full-scale char combustor operation.

The model calculates overall carbon burnout as a function of particle residence time. It assumes that the coal particles are uniformly mixed throughout the flow cross section and are fully entrained by the gas. One-dimensional plug flow is also assumed. Both shrinking-core and

constant-core particle combustion models are included. In the shrinking-core model, the char burns with steadily decreasing size, but at constant density. In the constant-core model, the char burns with steady reduction in density (pore enlargement), but at constant size. The calculations presented here represent the shrinking-core case, which in general yields a lower (more conservative) burnout rate and is also more appropriate for high-temperature char oxidation in which the surface kinetic rates are nearly equal to the corresponding bulk diffusion rates.

Inputs to the model include initial carbon content (following devolatilization), char particle size distribution, and bulk gas temperatures and species concentrations as a function of overall burnout.

Figure 29 is a plot of calculated char burnout as a function of combustor residence time for combustor operating conditions representative of TRW's Cleveland Demonstration Plant. The plot shows the effect of coal volatile content on calculated and measured carbon burnout. The air temperature at the inlet of the precombustor was approximately 350°F, while the combustor stoichiometry was 0.8 (fuel rich). For this combustor (40 mm Btu/h rating), approximately 40 ms of residence time is available upstream of the slag baffle. For Ohio No. 6 coal, a high-volatile bituminous coal, predicted carbon burnout within this time was approximately 99 percent. Actual carbon burnout, as determined through a combination of stack gas, slag, and fly-ash analyses, was typically in the range of 99 to 100 percent. For Balcke-Durr coal, a German semi-anthracite with an ASTM volatile content of 8 percent, predicted burnout is 85 percent, which also agrees well with the measured range of burnout for this coal. Hence, at the 40 mm Btu/h combustor level, the coal volatile content has a significant effect on combustor performance, for the same values of air preheat temperature and combustor stoichiometry.

Note in Figure 29 that the level of carbon burnout is expected to increase for larger combustor sizes due to the longer residence time available. For example, a 320 mm Btu/h combustor will have approximately 3 to 4 times more residence time than the smaller, 40 mm Btu/h combustor. At the larger size, the effect of volatile content on carbon burnout is much less, with predicted burnouts of over 99 percent for both the high volatile Ohio No. 6 coal and the low volatile Balcke-Durr coal.

The effect of char particle size on carbon burnout for different combustor sizes is shown in Figure 30. For these calculations, combustor conditions expected for the HIPPS char combustor were assumed (air-inlet temperature of 1120°F, stoichiometry of 0.8). In addition, the combustion of Pittsburgh No. 8 char was modeled, with a ASTM volatile content of 2 to 4 percent, consistent with the char produced by the Foster Wheeler pyrolyzer. Three different char particle size distributions were considered, with 50, 70, and 90 percent of the char particles passing through a 200 mesh screen. The corresponding median particle sizes for these cases were 74, 47, and 27 micron, respectively.

As shown in Figure 30, the char particle size has a strong impact on carbon burnout, especially at short residence times. For combustor sizes of less than approximately 20 mm Btu/h, the carbon burnout is too low to adequately address combustor performance. In the range of 20 to 40 mm Btu/h, carbon burnouts of 95 percent and above can be achieved

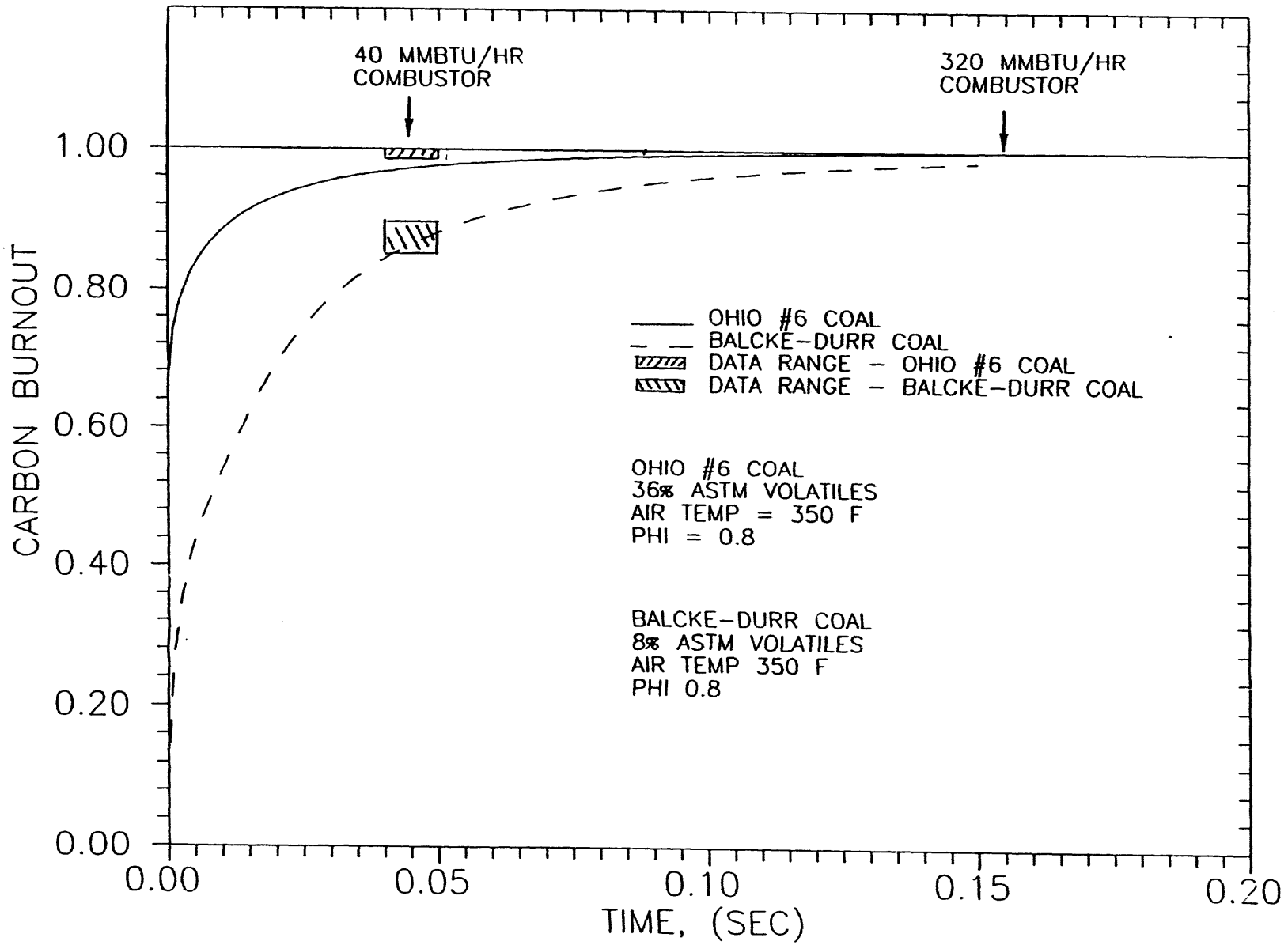

Figure 29 Effect of Volatile Content on Carbon Burnout

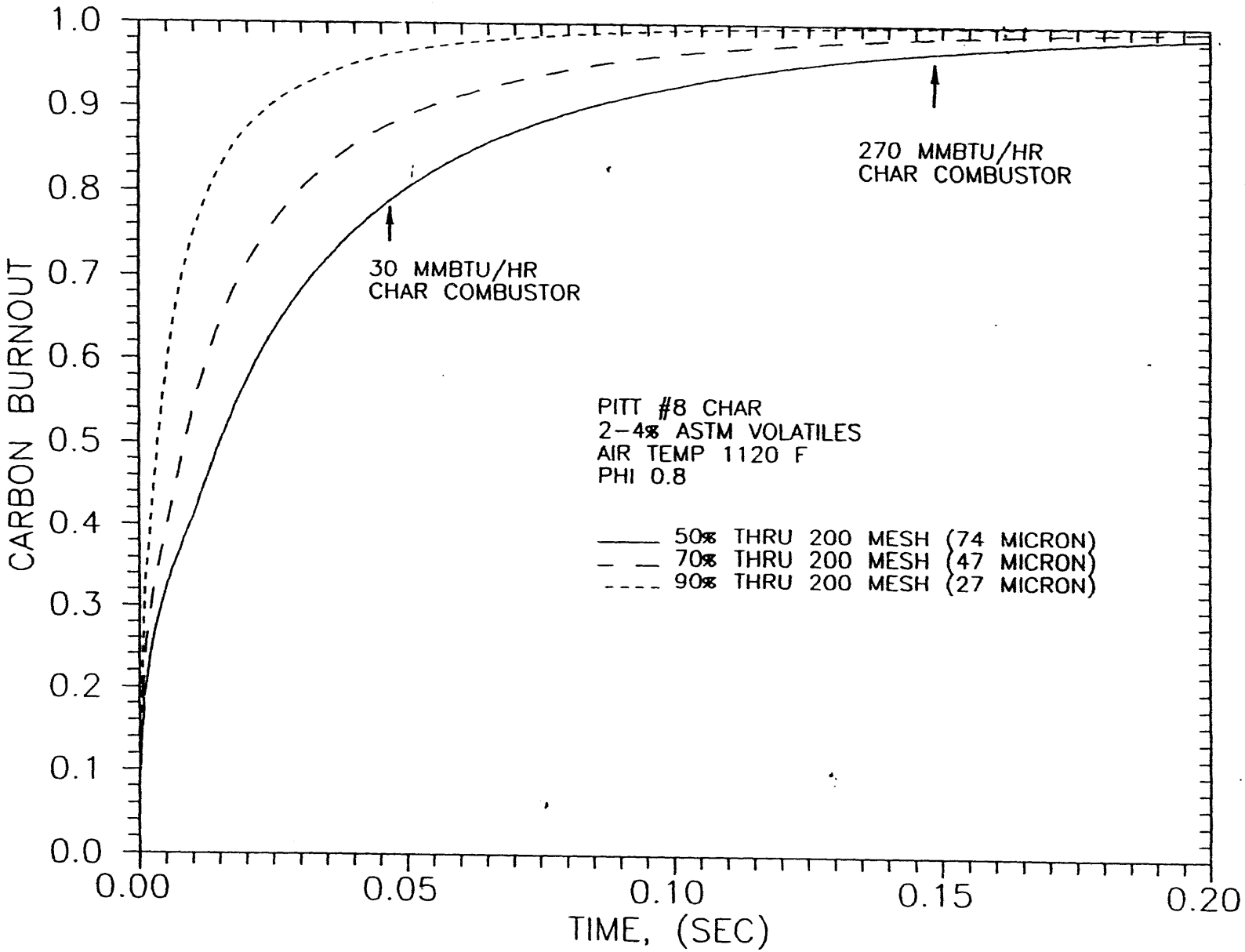

Figure 30 Effect of Char Particle Size on Carbon Burnout

Table 12 Base Case Emissions Analysis

INITIAL CONDITIONS	
COAL % ASH	10.32
COAL % S	2.99
Ca/S TO PYROLYZER	0.8
% SOLIDS TO FUEL GAS	/
% S TO H2S	5
COMBUST % ASH CAPT	80
COMBUST % S CAPT	20
BARRIER FILTER %	0
PART CONTROL %	99.8
DESOX %	95
DENOX1 %	50
DENOX2 %	0
% NH3 IN FUEL GAS	0.16
NH3 TO NO CONVERSION	25
FG COMB LB/MMBTU	0.34
PRECOMB LB/MMBTU	0.25
CHARCOM LB/MMBTU	0.25
GT COMB LB/MMBTU	0.2
VA COMB NOx RED %	50

SYSTEM EMISSION RATES	
LB/MM BTU SO2	0.1353
LB/MM BTU NOX	0.1335
LB/MM BTU ASH	0.0042
MM BTU/HR	2202
MW @ 48% EFF	310

HITAF FLOW CONDITIONS

STREAM NUMBER	FLOW K LB/HR	PRESS PSIA	TEMP DEG F	S LB/HR	NO LB/HR	PART LB/HR	HHV BTU/LB
1 COAL	110.3	50	60	3298.0	0.0	17319.3	12916
2 FUELGAS	373	30	1700	164.9	0.0	1212.4	2074
3 FLUEGAS	995	15	1900	164.9	263.3	1212.4	
4 NATGAS	27	250	200	0.0	0.0	0.0	23861
5 AIR	2911	191	1800	0.0	0.0	0.0	
6 VITAIR	3493	16	1100	0.0	128.8	0.0	
7 VITAIR	1588	16	1000	0.0	58.6	0.0	
8 VITAIR	1905	16	350	0.0	70.3	0.0	
9 VITAIR	1905	16	350	0.0	70.3	0.0	
10 CHAR	52.1	45	1700	3133.1	121.6	16107.0	9338
11 COAL	10.3	16	60	306.0	33.3	1063.0	12916
12 FLUEGAS	1717	15	300	2979.3	447.5	4646.3	
13 FLUEGAS	1717	15	300	2979.3	447.5	4646.3	
14 FLUEGAS	1717	15	300	2979.3	447.5	9.3	
15 FLUEGAS	1717	15	100	149.0	223.7	9.3	
16 STACK	3622	15	100	149.0	294.0	9.3	

by using a fine grind, which will provide an acceptable simulation of the combustor performance at larger sizes. Using a fine grind for sub-scale testing also makes sense for the purpose of preserving relative particle trajectories, since cyclonic efficiency is roughly preserved by maintaining the ratio of particle diameter squared to the combustor diameter.

Note in Figure 30 that carbon burnout levels of over 99 percent are predicted for a 270 mm Btu/h combustor for a char size of 70 percent through 200 mesh or finer. This is the combustor firing rate projected for the 290-MW plant. Note also that at this combustor size, the effect of particle size is much less. More detailed char oxidation calculations with the multizone combustor model are planned during the next quarter to confirm these results.

REFERENCES

1. "Development of a High-Performance Coal-Fired Power Generating System With Pyrolysis Gas and Char-Fired High-Temperature Furnace (HITAF)—Quarterly Report 5 (January through March 1993)," May 1993, pp. 17-19.

2. "Development of a High-Performance Coal-Fired Power Generating System With Pyrolysis Gas and Char-Fired High-Temperature Furnace (HITAF)—Quarterly Report 2 (April through June 1992)," July 1992.

3. T. R. Thompson, et al., "Application of High-Temperature Air Heaters To Advanced Power Generation Cycles." Proceedings of the American Power Conference, April 1992.

4. N. S. Jacobson, et al., "Molten Salt Corrosion of SiC and Si_3N_4," Handbook of Ceramics and Composites, Vol. 1, 1990, pp. 99-136.

5. M. K. Ferber and V. J. Tennery, "Evaluation of Tubular Ceramic Heat Exchanger Materials in Basic Coal Ash From Coal-Oil-Mixture Combustion," DOE Contract No. W-7405-eng-26 with Union Carbide, October 1982.

6. W. A. Kern, R. E. Tressler, and M. J. McNallen, "Durability of SiC/Al_2O_3 Composites in Contact with Sodium Silicate," Center for Advanced Materials Newsletter, Vol. 6, 1992, pp. 1-6.

7. A. Robertson, et al., "Second-Generation Pressurized Fluidized Bed Combustion Plant—Conceptual Design of a Second-Generation PFB Combustion Plant, Phase 1 Task 1, Vol. 3, Appendix C," DOE Contract DE-AC21-86MC21023, September 1989, pp. C-104 to C-107.

8. "Development of a High-Performance Coal-Fired Power Generating System With Pyrolysis Gas and Char-Fired High-Temperature Furnace (HITAF)—Quarterly Report 3 (July through October 1992)," November 1992, pp. 8-10.

9. M. G. Alliston, "The Integration of System Parameters in the Modeling of CFB Solids and Carbon Behavior," Proceedings of the 1989 International Conference on Fluidized Bed Combustion, pp. 31-36.

10. American Petroleum Institute Publication 931, Chapter 11—Cyclone Separators, May 1975.

11. "Development of a High-Performance Coal-Fired Power Generating System With Pyrolysis Gas and Char-Fired High-Temperature Furnace (HITAF)—Quarterly Report 4 (October through December 1992), February 1993, pp. 50-54.

12. R. H. Hurt and R. E. Mitchell, "Unified High-Temperature Char Combustion Kinetics for a Suite of Coals of Various Rank," 24th Symposium (International) on Combustion, The Combustion Institute, Pittsburgh, PA (1992).

13. R. H. Hurt, R. E. Mitchell, L. L. Baxter, and D. R. Hardesty, "Char Combustion Kinetics of U. S. Coals: A Comprehensive Data Base for Industry," Proceedings of the Ninth Annual Pittsburgh Coal Conference, Pittsburgh, PA, 1992, pp. 634-639.

14. R. H. Hurt, Personal Communication, 1993.

15. "Development of a High-Performance Coal-Fired Power Generating System With Pyrolysis Gas and Char-Fired High-Temperature Furnace (HITAF)—Quarterly Report 5 (January through March 1993), May 1993, pp. 46-52.

16. S. J. Priebe, et al., "An Assessment of Nitrogen Oxide Formation in Preheated High-Temperature Combustion Air in Industrial Processes," Report of Work Performed Under DOE Contract DE-AC07-761D01570, September 1986.

17. "Development of a High-Performance Coal-Fired Power Generating System With Pyrolysis Gas and Char-Fired High-Temperature Furnace (HITAF)—Quarterly Report 4 (October through December 1992), February 1993, pp. 67-72.

DATE FILMED

1 / 5 / 94

END